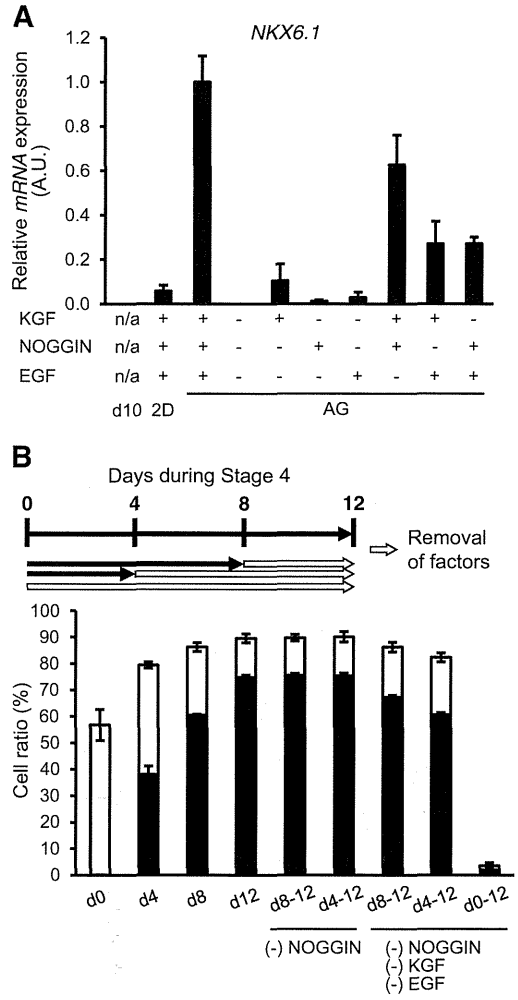

Figure 5 Both cell aggregation cultures and soluble factor treatment are required for the efficient induction of PDX1$^+$NKX6.1$^+$ cells. (A) *NKX6.1* expression was assessed by qRT-PCR in the cells treated with various combinations of soluble factors (100 ng/ml KGF, 100 ng/ml NOGGIN and 50 ng/ml EGF) for four days of Stage 4 aggregation culture. Cell aggregation alone did not induce the expression of *NKX6.1*. Treatment with all soluble factors with aggregation cultures most potently induced the expression of *NKX6.1*. (B) NOGGIN or all of the soluble factors (KGF, NOGGIN and EGF) was/were removed at the indicated periods during 12 days of aggregation culture at Stage 4. (Upper) A schematic diagram of the procedures used to assess the specific timing requirements for the soluble factors. (Lower) The quantification of the induction rate of PDX1$^+$NKX6.1$^+$ (black bars) and PDX1$^+$NKX6.1$^-$ (white bars) cells. The data are from three independent experiments presented as the mean ± S.E.M. n/a, not applicable.

that there was an about 10% increase in the NKX6.1$^+$ cell ratio by pre-treatment with the ALK5 inhibitor (data not shown). The human C-peptide levels in mouse plasma were gradually increased over time (Fig. 7A), and human C-peptide was detected in 11 out of 13 mice by 150 days after implantation (one mouse died before day 150). We found a similar tendency for a gradual increase in the human C-peptide levels in mice that underwent the implantation of cellular aggregates without the pre-treatment with an ALK5 inhibitor (data not shown). Moreover, we obtained grafts which were capable of responding to the changes in blood glucose levels by 150 days (Fig. 7B). There were also islet-like INS$^+$ cell clusters found inside the grafts, which did not co-express GCG on day 210 after implantation (Fig. 7C). These results suggest that the pancreatic cells generated with aggregation cultures have the developmental potential to differentiate into pancreatic epithelia and mature into β-cells *in vivo*.

Discussion

It has recently been demonstrated that hESCs/iPSCs can be differentiated into pancreatic lineages that show therapeutic potential for diabetes (Rezania et al., 2012, 2013; Bruin et al., 2013). Although the inducing factors have been intensively explored, the most suitable conditions to generate pancreatic cells have not yet been fully established. The obstacles preventing the establishment of such conditions include the different propensities for directed differentiation among hESC/iPSC lines (Osafune et al., 2008). We herein demonstrated that aggregation cultures efficiently induced the differentiation of pancreatic bud cells in multiple hESC/iPSC lines.

During embryonic development, the lineage commitment into the pancreas occurs at the step of pancreatic bud formation, in which Pdx1$^+$ cells form clusters and start expressing Ptf1a and Nkx6.1. A previous report utilized a rotational suspension-based differentiation method to generate PDX1$^+$NKX6.1$^+$ pancreatic bud progenitors from a hESC line, CyT49 (Schulz et al., 2012). Their use of cell aggregation cultures throughout the differentiation process from the undifferentiated state resulted in the efficient induction of PDX1$^+$NKX6.1$^+$ cells. Consistent with that study, we found that a higher cell density led to more efficient generation of PDX1$^+$NKX6.1$^+$ cells. Although the current model does not directly address the molecules responsible for these findings, the previous works and our current study allow us to hypothesize that a high cell density acts as a factor to activate the essential signals for the differentiation of posterior foregut cells into pancreatic bud.

Our findings suggest that the signals elicited by a high cell density or their surrogate stimuli are potent inducers of the directed differentiation of hESCs/iPSCs into pancreatic lineages. The efficient generation of PDX1$^+$NKX6.1$^+$ cells with adherent culture conditions in another report (Rezania et al., 2012) may have resulted from the acquisition of the signals due to the culture conditions or because the cell lines used intrinsically possessed the signals. Indeed, the increased cell number observed in Stage 1 resulted in a higher cell density at Stage 4, thus producing more efficient induction of NKX6.1$^+$ cells in the adherent cultures without re-seeding at Stage 4 (S4F; Supplementary Table 3). This result supports the idea that a high cell density is a key factor for pancreatic bud induction. We reason that unknown factors, including cell density factors, acting at specific times explain the variation in the differentiation efficiency noted in the different research groups. In the

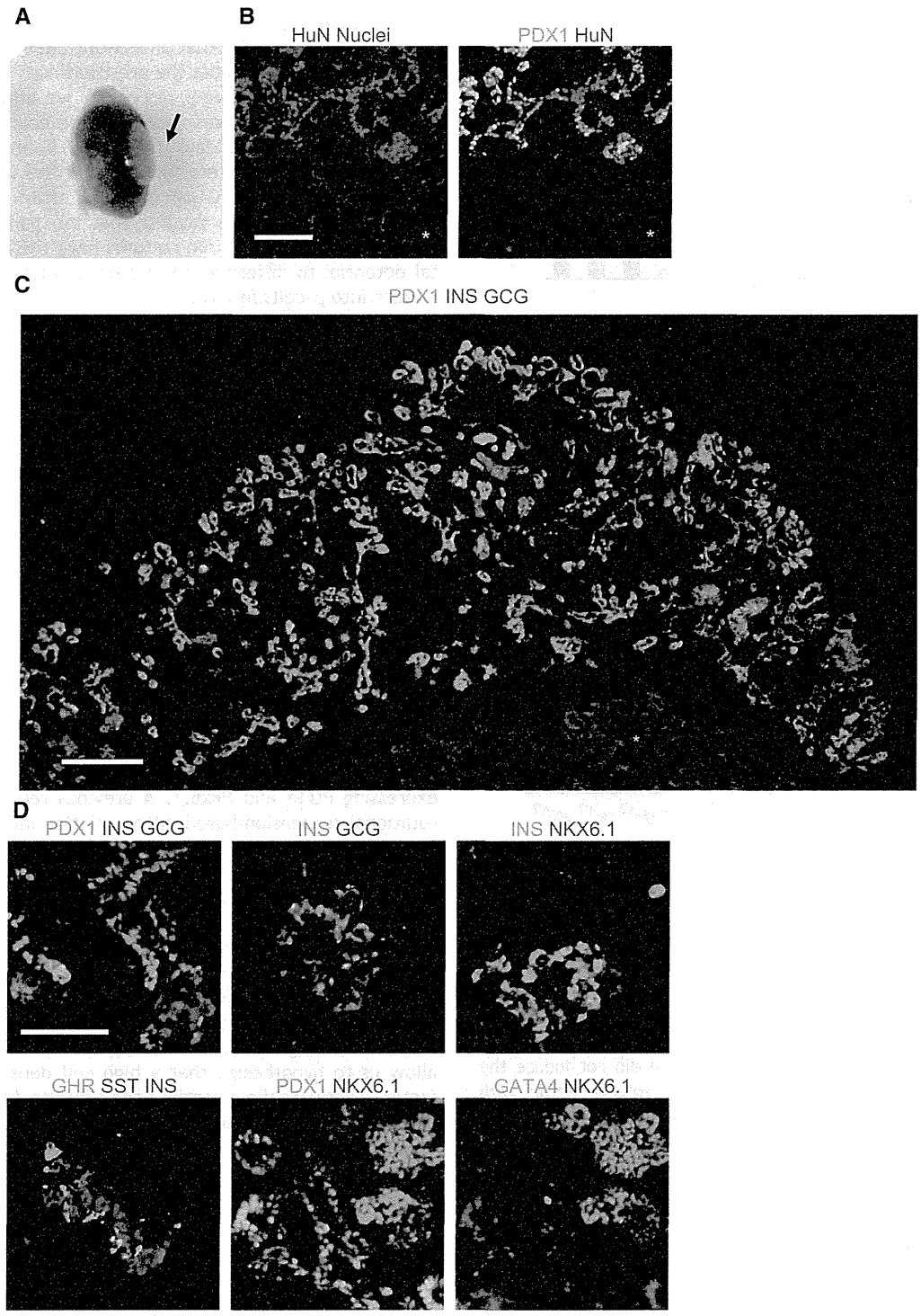

Figure 6 The PDX1^{+}NKX6.1^{+} cells generated with aggregation cultures differentiate into branched pancreatic epithelia *in vivo*. Cellular aggregates at Stage 4, days 4–5, were implanted into the kidney subcapsules of NOD–SCID mice. (A) An image of a host kidney harvested 30 days after implantation. The arrow indicates the location of the graft. (B–D) Cryosections of grafts were stained for the indicated markers. Representative images of human pancreatic cells are shown. Asterisks indicate the host mouse kidney in B and C. HuN, human nuclei. Scale bars, 100 μm in B and D and 300 μm in C.

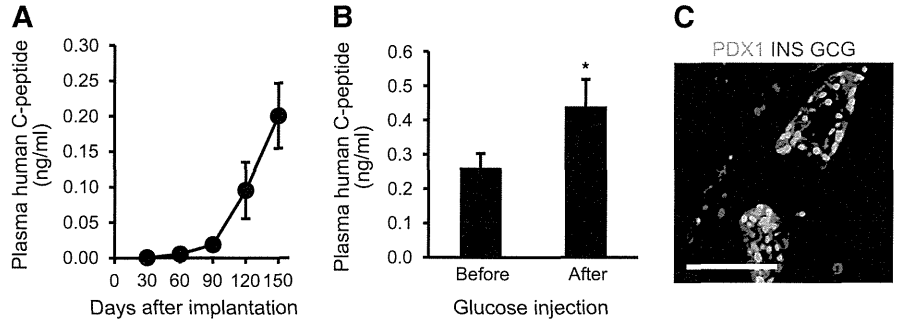

Figure 7 The PDX1$^+$NKX6.1$^+$ cells generated with aggregation cultures mature into functional β-cells *in vivo*. A total of six million cells at Stage 4, day 5, of aggregation cultures that had been pre-treated with an ALK5 inhibitor were implanted under the kidney subcapsule of NOD–SCID mice. (A) The average plasma human C-peptide levels in host mice were measured 30 min after glucose injection (3.0 g/ kg body weight, i.p.) at various time points after implantation, as indicated. (B) The average plasma human C-peptide levels after >5 h of fasting (before) and 30 min after glucose injection (after) in the host mice were examined on day 150 after implantation. (C) A representative image of hESC-derived islet-like endocrine clusters on day 210 after implantation. The data are presented as the mean ± S.E.M. of 13 mice from four independent cohorts of implantation experiments in A and four mice from two independent cohorts of implantation experiments in B. *$P < 0.05$. Scale bar, 100 μm.

present study, the induction rates of PDX1$^+$NKX6.1$^+$ cells were lower with some cell lines than with a hESC line, KhES-3. One plausible explanation is the low induction efficiency of cells in the steps before aggregation formation, such as definitive endoderm or posterior foregut cells. The optimization of culture conditions for these steps could make further contributions to resolving the problems of line-to-line variation of hESCs/iPSCs.

Although the detailed mechanisms underlying the increase in PDX1$^+$NKX6.1$^+$ cell induction in aggregation cultures remain unknown, this finding raises the possibility that pancreatic bud formation may be regulated by the molecules associated with contact-dependent cellular interactions, such as extracellular matrices and adhesion molecules, and other membrane-bound receptors (Brafman et al., 2013; Crisera et al., 2000; Ekblom et al., 1998). Possible mechanisms include the involvement of laminin–integrin signaling. During pancreatic development, epithelial cell delamination and migration into mesenchyme is the early event in the differentiation process into endocrine cells (Villasenor et al., 2012). However, we found that the expression levels of pan-laminin were similar between NKX6.1$^+$ cells and NKX6.1$^-$ cells in both aggregation and monolayer cultures (data not shown). Although we could not exclude the possibility that laminin isoforms are different between the cell populations, we assumed that typical laminin–integrin signals are not likely to be directly involved. In addition, based on the findings obtained with the other extracellular matrices (Fig. S1), at a minimum, laminin-111, vitronectin (main component of Synthemax), fibronectin and collagen I are not likely to be involved. Instead, other cell surface-derived signals, such as those associated with the apicobasal polarity (Villasenor et al., 2010; Kesavan et al., 2009) and planar cell polarity pathways (Cortijo et al., 2012), or unknown autocrine/paracrine molecules, may be involved. Further studies with comparative analyses of the gene expression profiles between 2D and aggregation cultures would be helpful to elucidate the factors responsible for the regulation of NKX6.1 induction in developing pancreatic buds.

It is possible that the signals elicited by a high cell density increased the ratio of PDX1$^+$NKX6.1$^+$ cells *via* the direct induction of differentiation into PDX1$^+$NKX6.1$^+$ cells, while the selective proliferation of progenitor cells and/or selective apoptosis of uncommitted cells are also possible mechanisms. The number of proliferating cells was low on days 1–2 in Stage 4, during which time the PDX1$^+$NKX6.1$^+$ cells emerged in the cell aggregation cultures (Figs. S5A and C). In addition, the total cell number in the aggregation cultures was not increased at Stage 4, days 1–2, suggesting the involvement of selective proliferation to be less likely (Fig. S3). On the other hand, the number of apoptotic cells was increased in the cellular aggregates, consistent with the idea that aggregation cultures selectively delete cells uncommitted to the PDX1$^+$NKX6.1$^+$ cell lineage (Figs. S5B and D). In fact, more apoptotic cells were found within the PDX1$^-$ cell population (Fig. S5D), which suggests that selective apoptosis is a possible mechanism. In the future, the identification of marker genes for pancreatic cells uncommitted to NKX6.1$^+$ cells and application of subsequent live cell imaging with the reporter cell line of the marker would help to clearly demonstrate the involvement of selective apoptosis in the increased PDX1$^+$NKX6.1$^+$ cell ratio observed in high-density cultures.

It was previously reported that the activation of BMP signaling facilitates the proliferation of NKX6.1$^+$ cells (Sui et al., 2013). In contrast, our data indicate that the inhibition by adding NOGGIN increased the *NKX6.1* expression (Fig. 5A). Consistent with our findings, other reports have demonstrated that NKX6.1$^+$ pancreatic progenitors were generated under continuous suppression of BMP signaling in hESC differentiation cultures (Rezania et al., 2012, 2013; Schulz et al., 2012; Bruin et al., 2013), and that the phosphorylation of smad1/5/8, downstream effectors of BMP signaling, was suppressed in Nkx6.1$^+$ cells from developing chick pancreatic buds (Ahnfelt-Ronne et al., 2010). In addition, the BMP inhibition by *in ovo* gene transfer of Noggin into the presumptive pancreatic region of chick embryos resulted in pancreatic bud formation without further branching and epithelialization (Ahnfelt-Ronne et al., 2010). We reasoned that BMP inhibition

is involved in the commitment to NKX6.1$^+$ cells, but that BMP signaling is necessary for the subsequent proliferation and differentiation. In agreement with this, we found that the induction rate of PDX1$^+$NKX6.1$^+$ cells was continuously increased with the removal of NOGGIN after day 4 of Stage 4 (Fig. 5B). Although BMP activation may expand NKX6.1$^+$ cells, we assume that the first four days of aggregation cultures are critical for the commitment of PDX1$^+$NKX6.1$^+$ cells, and that all three factors are beneficial for the PDX1$^+$NKX6.1$^+$ cell induction.

In summary, the cell density of PDX1$^+$ posterior foregut cells positively correlates with the induction of PDX1$^+$NKX6.1$^+$ pancreatic bud cells in hESC/iPSC differentiation cultures. Although the molecules that regulate the differentiation step remain unknown, the signals elicited by high cell density are crucial for the pancreatic bud induction, and synergistically work with soluble factors. To our knowledge, this is the first study clearly demonstrating that the signals derived from spatial and morphological contexts are associated with the differentiation of hESCs/iPSCs into pancreatic lineages. Further studies to elucidate the molecular nature of the signals based on our findings may contribute to the development of hESC/iPSC-based cell therapy for diabetes.

Supplementary data to this article can be found online at http://dx.doi.org/10.1016/j.scr.2015.01.007.

Acknowledgments

This work was supported in part by funding from the Takeda Science Foundation to T.T., the Suzuken Memorial Foundation to T.T. and the Life Science Foundation of Japan to K.O., by the Japan Society for the Promotion of Science (JSPS) through its 'Funding Programme for World-Leading Innovative R&D on Science and Technology (FIRST Programme)' to K.O. and Grant-in-Aid for Young Scientists (B) to T.T. and by the Japan Science and Technology Agency (JST) through its research grant "Core Center for iPS Cell Research and Projects for Technological Development, Research Center Network for Realization of Regenerative Medicine" to Y.K. and K.O. T.T. wrote the first draft of the manuscript. T.T., S.M., Y.K. and K.O. contributed to manuscript edits and revisions. T.T., S.M., Y.K., M.F., Y.H., Y.K. and K.O. designed, directed, and interpreted the experiments. T.T., S.M., H.T. and T.S. performed the experiments. K.O. supervised the study. The authors thank Kanae Mitsunaga for her technical assistance in the flow cytometry analysis and Yasuhiro Nakano for providing valuable advice on this research.

References

Ahnfelt-Ronne, J., Ravassard, P., Pardanaud-Glavieux, C., Scharfmann, R., Serup, P., 2010. Mesenchymal bone morphogenetic protein signaling is required for normal pancreas development. Diabetes 59, 1948–1956.

Ahnfelt-Ronne, J., Jorgensen, M.C., Klinck, R., Jensen, J.N., Fuchtbauer, E.M., Deering, T., MacDonald, R.J., Wright, C.V., Madsen, O.D., Serup, P., 2012. Ptf1a-mediated control of Dll1 reveals an alternative to the lateral inhibition mechanism. Development 139, 33–45.

Brafman, D.A., Phung, C., Kumar, N., Willert, K., 2013. Regulation of endodermal differentiation of human embryonic stem cells through integrin–ECM interactions. Cell Death Differ. 20, 369–381.

Bruin, J.E., Rezania, A., Xu, J., Narayan, K., Fox, J.K., O'Neil, J.J., Kieffer, T.J., 2013. Maturation and function of human embryonic stem cell-derived pancreatic progenitors in macroencapsulation devices following transplant into mice. Diabetologia 56, 1987–1998.

Cai, J., Yu, C., Liu, Y., Chen, S., Guo, Y., Yong, J., Lu, W., Ding, M., Deng, H., 2010. Generation of homogeneous PDX1(+) pancreatic progenitors from human ES cell-derived endoderm cells. J. Mol. Cell Biol. 2, 50–60.

Cortijo, C., Gouzi, M., Tissir, F., Grapin-Botton, A., 2012. Planar cell polarity controls pancreatic beta cell differentiation and glucose homeostasis. Cell Rep. 2, 1593–1606.

Crisera, C.A., Kadison, A.S., Breslow, G.D., Maldonado, T.S., Longaker, M.T., Gittes, G.K., 2000. Expression and role of laminin-1 in mouse pancreatic organogenesis. Diabetes 49, 936–944.

D'Amour, K.A., Bang, A.G., Eliazer, S., Kelly, O.G., Agulnick, A.D., Smart, N.G., Moorman, M.A., Kroon, E., Carpenter, M.K., Baetge, E.E., 2006. Production of pancreatic hormone-expressing endocrine cells from human embryonic stem cells. Nat. Biotechnol. 24, 1392–1401.

Dominguez-Bendala, J., Inverardi, L., Ricordi, C., 2011. Stem cell-derived islet cells for transplantation. Curr. Opin. Organ Transplant. 16, 76–82.

Donath, M.Y., Halban, P.A., 2004. Decreased beta-cell mass in diabetes: significance, mechanisms and therapeutic implications. Diabetologia 47, 581–589.

Ekblom, M., Falk, M., Salmivirta, K., Durbeej, M., Ekblom, P., 1998. Laminin isoforms and epithelial development. Ann. N. Y. Acad. Sci. 857, 194–211.

Fukuda, A., Kawaguchi, Y., Furuyama, K., Kodama, S., Kuhara, T., Horiguchi, M., Koizumi, M., Fujimoto, K., Doi, R., Wright, C.V., Chiba, T., 2006. Loss of the major duodenal papilla results in brown pigment biliary stone formation in pdx1 null mice. Gastroenterology 130, 855–867.

Hald, J., Sprinkel, A.E., Ray, M., Serup, P., Wright, C., Madsen, O.D., 2008. Generation and characterization of Ptf1a antiserum and localization of Ptf1a in relation to Nkx6.1 and Pdx1 during the earliest stages of mouse pancreas development. J. Histochem. Cytochem. 56, 587–595.

Jennings, R.E., Berry, A.A., Kirkwood-Wilson, R., Roberts, N.A., Hearn, T., Salisbury, R.J., Blaylock, J., Piper Hanley, K., Hanley, N.A., 2013. Development of the human pancreas from foregut to endocrine commitment. Diabetes 62, 3514–3522.

Jensen, J., 2004. Gene regulatory factors in pancreatic development. Dev. Dyn. 229, 176–200.

Jiang, W., Shi, Y., Zhao, D., Chen, S., Yong, J., Zhang, J., Qing, T., Sun, X., Zhang, P., Ding, M., Li, D., Deng, H., 2007a. In vitro derivation of functional insulin-producing cells from human embryonic stem cells. Cell Res. 17, 333–344.

Jiang, J., Au, M., Lu, K., Eshpeter, A., Korbutt, G., Fisk, G., Majumdar, A.S., 2007b. Generation of insulin-producing islet-like clusters from human embryonic stem cells. Stem Cells 25, 1940–1953.

Jorgensen, M.C., Ahnfelt-Ronne, J., Hald, J., Madsen, O.D., Serup, P., Hecksher-Sorensen, J., 2007. An illustrated review of early pancreas development in the mouse. Endocr. Rev. 28, 685–705.

Kajiwara, M., Aoi, T., Okita, K., Takahashi, R., Inoue, H., Takayama, N., Endo, H., Eto, K., Toguchida, J., Uemoto, S., Yamanaka, S., 2012. Donor-dependent variations in hepatic differentiation from human-induced pluripotent stem cells. Proc. Natl. Acad. Sci. U. S. A. 109, 12538–12543.

Kawaguchi, Y., Cooper, B., Gannon, M., Ray, M., MacDonald, R.J., Wright, C.V., 2002. The role of the transcriptional regulator Ptf1a in converting intestinal to pancreatic progenitors. Nat. Genet. 32, 128–134.

Kelly, O.G., Chan, M.Y., Martinson, L.A., Kadoya, K., Ostertag, T.M., Ross, K.G., Richardson, M., Carpenter, M.K., D'Amour, K.A., Kroon, E., Moorman, M., Baetge, E.E., Bang, A.G., 2011. Cell-surface markers for the isolation of pancreatic cell types derived from human embryonic stem cells. Nat. Biotechnol. 29, 750–756.

Kesavan, G., Sand, F.W., Greiner, T.U., Johansson, J.K., Kobberup, S., Wu, X., Brakebusch, C., Semb, H., 2009. Cdc42-mediated tubulogenesis controls cell specification. Cell 139, 791–801.

Kroon, E., Martinson, L.A., Kadoya, K., Bang, A.G., Kelly, O.G., Eliazer, S., Young, H., Richardson, M., Smart, N.G., Cunningham, J., Agulnick, A.D., D'Amour, K.A., Carpenter, M.K., Baetge, E.E., 2008. Pancreatic endoderm derived from human embryonic stem cells generates glucose-responsive insulin-secreting cells in vivo. Nat. Biotechnol. 26, 443–452.

Kunisada, Y., Tsubooka-Yamazoe, N., Shoji, M., Hosoya, M., 2012. Small molecules induce efficient differentiation into insulin-producing cells from human induced pluripotent stem cells. Stem Cell Res. 8, 274–284.

Mae, S., Shono, A., Shiota, F., Yasuno, T., Kajiwara, M., Gotoda-Nishimura, N., Arai, S., Sato-Otubo, A., Toyoda, T., Takahashi, K., Nakayama, N., Cowan, C.A., Aoi, T., Ogawa, S., McMahon, A.P., Yamanaka, S., Osafune, K., 2013. Monitoring and robust induction of nephrogenic intermediate mesoderm from human pluripotent stem cells. Nat. Commun. 4, 1367.

Mathis, D., Vence, L., Benoist, C., 2001. Beta-cell death during progression to diabetes. Nature 414, 792–798.

Matsumoto, S., 2011. Clinical allogeneic and autologous islet cell transplantation: update. Diabetes Metab. J. 35, 199–206.

McCall, M.D., Toso, C., Baetge, E.E., Shapiro, A.M., 2010. Are stem cells a cure for diabetes? Clin. Sci. (Lond.) 118, 87–97.

Mfopou, J.K., Chen, B., Mateizel, I., Sermon, K., Bouwens, L., 2010. Noggin, retinoids, and fibroblast growth factor regulate hepatic or pancreatic fate of human embryonic stem cells. Gastroenterology 138, 2233–2245 (2245 e2231–2214).

Nostro, M.C., Sarangi, F., Ogawa, S., Holtzinger, A., Corneo, B., Li, X., Micallef, S.J., Park, I.H., Basford, C., Wheeler, M.B., Daley, G.Q., Elefanty, A.G., Stanley, E.G., Keller, G., 2011. Stage-specific signaling through TGFbeta family members and WNT regulates patterning and pancreatic specification of human pluripotent stem cells. Development 138, 861–871.

Okita, K., Matsumura, Y., Sato, Y., Okada, A., Morizane, A., Okamoto, S., Hong, H., Nakagawa, M., Tanabe, K., Tezuka, K., Shibata, T., Kunisada, T., Takahashi, M., Takahashi, J., Saji, H., Yamanaka, S., 2011. A more efficient method to generate integration-free human iPS cells. Nat. Methods 8, 409–412.

Osafune, K., Caron, L., Borowiak, M., Martinez, R.J., Fitz-Gerald, C.S., Sato, Y., Cowan, C.A., Chien, K.R., Melton, D.A., 2008. Marked differences in differentiation propensity among human embryonic stem cell lines. Nat. Biotechnol. 26, 313–315.

Oster, A., Jensen, J., Serup, P., Galante, P., Madsen, O.D., Larsson, L.I., 1998. Rat endocrine pancreatic development in relation to two homeobox gene products (Pdx-1 and Nkx 6.1). J. Histochem. Cytochem. 46, 707–715.

Pan, F.C., Bankaitis, E.D., Boyer, D., Xu, X., Van de Casteele, M., Magnuson, M.A., Heimberg, H., Wright, C.V., 2013. Spatiotemporal patterns of multipotentiality in Ptf1a-expressing cells during pancreas organogenesis and injury-induced facultative restoration. Development 140, 751–764.

Rezania, A., Riedel, M.J., Wideman, R.D., Karanu, F., Ao, Z., Warnock, G.L., Kieffer, T.J., 2011. Production of functional glucagon-secreting alpha-cells from human embryonic stem cells. Diabetes 60, 239–247.

Rezania, A., Bruin, J.E., Riedel, M.J., Mojibian, M., Asadi, A., Xu, J., Gauvin, R., Narayan, K., Karanu, F., O'Neil, J.J., Ao, Z., Warnock, G.L., Kieffer, T.J., 2012. Maturation of human embryonic stem cell-derived pancreatic progenitors into functional islets capable of treating pre-existing diabetes in mice. Diabetes 61, 2016–2029.

Rezania, A., Bruin, J.E., Xu, J., Narayan, K., Fox, J.K., O'Neil, J.J., Kieffer, T.J., 2013. Enrichment of human embryonic stem cell-derived NKX6.1-expressing pancreatic progenitor cells accelerates the maturation of insulin-secreting cells in vivo. Stem Cells 31, 2432–2442.

Riedel, M.J., Asadi, A., Wang, R., Ao, Z., Warnock, G.L., Kieffer, T.J., 2012. Immunohistochemical characterisation of cells co-producing insulin and glucagon in the developing human pancreas. Diabetologia 55, 372–381.

Schulz, T.C., Young, H.Y., Agulnick, A.D., Babin, M.J., Baetge, E.E., Bang, A.G., Bhoumik, A., Cepa, I., Cesario, R.M., Haakmeester, C., Kadoya, K., Kelly, J.R., Kerr, J., Martinson, L.A., McLean, A.B., Moorman, M.A., Payne, J.K., Richardson, M., Ross, K.G., Sherrer, E.S., Song, X., Wilson, A.Z., Brandon, E.P., Green, C.E., Kroon, E.J., Kelly, O.G., D'Amour, K.A., Robins, A.J., 2012. A scalable system for production of functional pancreatic progenitors from human embryonic stem cells. PLoS One 7, e37004.

Serup, P., Petersen, H.V., Pedersen, E.E., Edlund, H., Leonard, J., Petersen, J.S., Larsson, L.I., Madsen, O.D., 1995. The homeodomain protein IPF-1/STF-1 is expressed in a subset of islet cells and promotes rat insulin 1 gene expression dependent on an intact E1 helix–loop–helix factor binding site. Biochem. J. 310 (Pt 3), 997–1003.

Shim, J.H., Kim, S.E., Woo, D.H., Kim, S.K., Oh, C.H., McKay, R., Kim, J.H., 2007. Directed differentiation of human embryonic stem cells towards a pancreatic cell fate. Diabetologia 50, 1228–1238.

Suemori, H., Yasuchika, K., Hasegawa, K., Fujioka, T., Tsuneyoshi, N., Nakatsuji, N., 2006. Efficient establishment of human embryonic stem cell lines and long-term maintenance with stable karyotype by enzymatic bulk passage. Biochem. Biophys. Res. Commun. 345, 926–932.

Sui, L., Geens, M., Sermon, K., Bouwens, L., Mfopou, J.K., 2013. Role of BMP signaling in pancreatic progenitor differentiation from human embryonic stem cells. Stem Cell Rev. 9, 569–577.

Villasenor, A., Chong, D.C., Henkemeyer, M., Cleaver, O., 2010. Epithelial dynamics of pancreatic branching morphogenesis. Development 137, 4295–4305.

Villasenor, A., Marty-Santos, L., Dravis, C., Fletcher, P., Henkemeyer, M., Cleaver, O., 2012. EphB3 marks delaminating endocrine progenitor cells in the developing pancreas. Dev. Dyn. 241, 1008–1019.

Xu, X., Browning, V.L., Odorico, J.S., 2011. Activin, BMP and FGF pathways cooperate to promote endoderm and pancreatic lineage cell differentiation from human embryonic stem cells. Mech. Dev. 128, 412–427.

Zhang, D., Jiang, W., Liu, M., Sui, X., Yin, X., Chen, S., Shi, Y., Deng, H., 2009. Highly efficient differentiation of human ES cells and iPS cells into mature pancreatic insulin-producing cells. Cell Res. 19, 429–438.

Journal of Neurochemistry JNC

JOURNAL OF NEUROCHEMISTRY | 2015 | 132 | 583–594 doi: 10.1111/jnc.13010

ORIGINAL ARTICLE

The extracellular fragment of GPNMB (Glycoprotein nonmelanosoma protein B, osteoactivin) improves memory and increases hippocampal GluA1 levels in mice

Kenta Murata,*[,1] Yuta Yoshino,*[,1] Kazuhiro Tsuruma,* Shigeki Moriguchi,† Atsushi Oyagi,* Hirotaka Tanaka,* Mitsue Ishisaka,* Masamitsu Shimazawa,* Kohji Fukunaga† and Hideaki Hara*

*Molecular Pharmacology, Department of Biofunctional Evaluation, Gifu Pharmaceutical University, Gifu, Japan

†Department of Pharmacology, Graduate School of Pharmaceutical Science, Tohoku University, Sendai, Japan

Abstract

Glycoprotein nonmelanoma protein B (GPNMB, *alias* osteoactivin), a type I transmembrane glycoprotein, is cleaved by extracellular proteases, resulting in release of an extracellular fragment (ECF). GPNMB is widely expressed by neurons within the CNS, including the hippocampus; however, its function in the brain remains unknown. Here, we investigated the role of GPNMB in memory and learning by using transgenic (Tg) mice over-expressing GPNMB (Tg mice on a BDF-1 background) and ECF-treated mice. In the hippocampus of both wild-type and Tg mice, GPNMB was highly expressed in neurons and astrocytes. Tg mice exhibited memory improvements in two types of learning tasks but were impaired in a passive-avoidance test. In Tg mice, the hippocampus displayed increased levels of the α-amino-3-hydroxy-5-methylisoxazole-4-propionate receptor subunit GluA1. Intracerebroventricular administration of ECF (50 ng) to Institute of Cancer Research (ICR) mice also improved memory in a passive-avoidance test and increased hippocampal GluA1 levels 24 h after treatment. In Tg mice and ECF (0.25 μg/mL)-treated hippocampal slices, long-term potentiation was promoted. These findings suggest that GPNMB may be a novel target for research on higher order brain functions.

Keywords: AMPA receptor subunit GluA1, Glycoprotein nonmelanosoma protein B (GPNMB), hippocampus, memory improvement, osteoactivin.

J. Neurochem. (2015) **132**, 583–594.

Glycoprotein nonmelanoma protein B (GPNMB, SWISS-PROT accession number Q14956) is a type I transmembrane glycoprotein consisting of three main domains: an N-terminal extracellular domain (amino acids 23–500), a transmembrane domain (amino acids 501–521), and a C-terminal intracellular domain (amino acids 522–572). GPNMB contains 13 *N*-linked glycosylation sites, a heparin-binding domain, an integrin-recognition Arg-Gly-Asp motif, and a polycystic kidney disease domain. Each of these domains performs specific roles (Ruoslahti 1996; Ogawa *et al.* 2005; Selim *et al.* 2007). Intact transmembrane GPNMB is cleaved by extracellular proteases, including matrix metalloproteinases (Furochi *et al.* 2007a) such as ADAM10 (a disintegrin and metalloproteinase domain-containing protein 10) (Rose *et al.* 2010), in a process called ectodomain shedding, which results in the release of the extracellular domain to act as a growth factor or cytokine (Huovila *et al.* 2005). This extracellular fragment (ECF) influences angiogenesis and the expression of other proteins (Ogawa *et al.* 2005; Rose

Received May 11, 2014; revised manuscript received November 22, 2014; accepted November 27, 2014.

Address correspondence and reprint requests to Prof Hideaki Hara, Department of Biofunctional Evaluation, Molecular Pharmacology, Gifu Pharmaceutical University, 1-25-4 Daigaku-nishi, Gifu 501-1196, Japan. E-mail: hidehara@gifu-pu.ac.jp

[1]These authors contributed equally to this work.

Abbreviations used: AMPA, α-amino-3-hydroxy-5-methylisoxazole-4-propionate; CaMK2, Ca^{2+}/calmodulin-dependent protein kinase 2; DG, dentate gyrus; GSK3β, glycogen synthase kinase 3β; NMDA, *N*-methyl-D-aspartate.

et al. 2010). *Gpnmb* mRNA and protein are widely expressed in, for example, liver, muscle, bone, and dendritic cells (Safadi *et al.* 2001; Haralanova-Ilieva *et al.* 2005; Ogawa *et al.* 2005; Schwarzbich *et al.* 2012). Recently, GPNMB has been reported to be expressed in neurons, microglia, and radial glia within the CNS, including the hippocampus, cerebral cortex, and spinal cord (Huang *et al.* 2012). Changes in GPNMB expression are observed in neurodegenerative diseases such as Parkinson's disease and amyotrophic lateral sclerosis (Plagnol *et al.* 2011; Tanaka *et al.* 2012). Animal models have been generated to facilitate investigation of the roles performed by GPNMB in various tissues. Transgenic mice over-expressing GPNMB were protected against motor neuron loss induced by a mutant superoxide dismutase ($SOD1^{G93A}$) (Tanaka *et al.* 2012), while DBA/2J mice possessing mutations in both *Gpnmb* and *tyrosinase-related protein 1* exhibited impaired hippocampus-dependent learning which was improved by treatment with aniracetam, an α-amino-3-hydroxy-5-methylisoxazole-4-propionate (AMPA) receptor modulator (Smith and Wehner 2002). However, little is known about the physiological functions of GPNMB, especially in the brain.

Glutamate, the major excitatory neurotransmitter in the mammalian CNS, activates several different types of receptor including *N*-methyl-D-aspartate (NMDA), AMPA, and metabotropic glutamate receptors. The AMPA receptor is a homotetramer or heterotetramer protein, with subunits termed GluA1–4. On induction of long-term potentiation (LTP) in hippocampal-slice preparations, GluA1-containing AMPA receptors are rapidly incorporated into synapses (Makino and Malinow 2009). Furthermore, synaptic GluA1 trafficking in the CA1 region of the hippocampus is required for memory encoding (Mitsushima *et al.* 2011). These reports suggest that GluA1 plays pivotal roles in synaptic plasticity and long-term memory. In the present study, we examined the roles performed by GPNMB in memory and learning by using transgenic (Tg) mice over-expressing GPNMB (Tg mice on a BDF-1 background) and by treating Institute of Cancer Research (ICR) mice with the ECF of GPNMB. In addition, using Tg and ECF-treated ICR mice, we evaluated GluA1 phosphorylation and expression, as well as the effects of GPNMB on LTP in hippocampal slices.

Materials and methods

Animals

GPNMB-over-expressing Tg mice were generated as described (Ogawa *et al.* 2005; Furochi *et al.* 2007b). Tg mice were established on a BDF-1 genetic background and were kindly gifted by Takeshi Nikawa MD (Tokushima University). For these experiments, we used male mice (10–15 weeks old) with wild-type (WT) littermates serving as the control group for the Tg mice. In addition, 6-week-old male ICR mice weighing 31–36 g were used; these were obtained from colonies of specific pathogen-free ICR mice maintained by Japan SLC (Shizuoka, Japan). All procedures relating to animal care and treatment conformed to animal care guidelines issued by the National Institutes of Health. Animals were housed in SPF conditions. All efforts were made to minimize both the suffering and the number of animals used. Animals were housed at 24 ± 2°C under a 12-h light–dark cycle (lights on from 8:00 to 20:00) and had access to food and water *ad libitum*. We used two strains of mice, BDF-1 and ICR. ICR mice were used in Figs 4(a), 5(a)–(d), 6(d)–(f), and Figure S5. BDF-1 mice were used to investigate the effect of GPNMB over-expression, which were described as WT and Tg. Independent groups were used in each behavioral trial.

Chemicals and drugs

Recombinant human osteoactivin/GPNMB, which has the same sequence as human GPNMB from Lys 23 to Asn 486, was purchased from R&D Systems (Minneapolis, MD, USA). The following chemicals and drugs were used: paraformaldehyde, sucrose, potassium chloride, methanol (Wako Pure Chemical, Osaka, Japan), isoflurane (Merk Hoei, Osaka, Japan), sodium hydrogen phosphate 12-water, sodium dihydrogen phosphate dehydrate (Nakarai Tesque, Kyoto, Japan), sodium chloride (Kishida Chemical, Osaka, Japan), sodium pentobarbital (Dainippon Pharmaceutical, Osaka, Japan), and Tissue-Tech OCT (Sakura Finetechnical, Tokyo, Japan).

Tissue preparation

Mice were anesthetized with sodium pentobarbital (50 mg/kg, intraperitoneal injection; i.p.) and perfused with saline until the outflow became clear, then immediately perfused with 4% paraformaldehyde for 10 min. Brains were removed and post-fixed in the same fixative for 24 h at 4°C. Brain sections were equilibrated in 25% sucrose solution and quickly frozen in Tissue-Tek OCT. Finally, 20-μm-thick sections of brain were cut on a cryostat.

Immunohistochemistry

The sections were stained with one of the following antibodies: goat anti-GPNMB polyclonal antibody (1 : 200; R&D Systems), mouse anti-NeuN monoclonal antibody (1 : 1000; Millipore, Billerica, MA, USA), mouse anti-glial fibrillary acidic protein (GFAP) monoclonal antibody (1 : 1000; Millipore), or rabbit anti-Iba-1 polyclonal antibody (1 : 200; Wako Pure Chemical). Sections were treated with 0.01 M phosphate-buffered saline (PBS) containing 1.5% normal horse serum for 1 h, and the anti-GPNMB antibody was applied overnight at 4°C. After washing with 0.01 M PBS, sections were blocked with mouse-on-mouse blocking reagent for 1 h at 20-26°C. After washing again with 0.01 M PBS, sections were incubated with anti-GFAP or anti-NeuN antibody overnight at 4°C. After further washing with 0.01 M PBS, immunoreactivity was visualized by incubation for 2 h at 20-26°C with the following secondary antibodies: Alexa Fluor 488 $F(ab')_2$ fragment of rabbit anti-mouse IgG (H+L) (1 : 1000; Invitrogen, Carlsbad, CA, USA), Alexa Fluor 546 $F(ab')_2$ fragment of rabbit anti-goat IgG (H+L) (1 : 1000; Invitrogen), Alexa Fluor 488 $F(ab')_2$ fragment of donkey anti-goat IgG (H+L) (1 : 1000; Invitrogen), or Alexa Fluor 546 $F(ab')_2$ fragment of donkey anti-rabbit IgG (H+L) (1 : 1000; Invitrogen).

Intracerebroventricular administration

Intracerebroventricular (i.c.v.) injections were performed −0.5 mm anteroposterior and 1.0 mm mediolateral to the bregma under isoflurane anesthesia. Anesthesia was induced with 0.3% isoflurane

(Escain; Mylan, Canonsburg, PA, USA) and maintained with 1.5% isoflurane in 70% N_2O and 30% O_2 via an animal general anesthesia machine (Soft Lander; Sin-ei Industry Co., Ltd., Saitama, Japan). A microliter syringe (Hamilton, Reno, NV, USA) was used for i.c.v. injections.

Morris water-maze test

The Morris water-maze test and novel object-recognition test were performed as previously described (Oyagi *et al.* 2009, 2012). A circular pool (diameter 120 cm × height 45 cm) was filled to a depth of 30 cm with water (21–23°C). Four equally spaced points around the edge of the pool were designated as the four starting positions. A hidden platform (diameter 10 cm) was set 0.5 cm below the surface of the water in a fixed position. A given mouse was placed in the water facing the wall and trained with four trials per day for 5 days. In each of a given day's four trials, a different starting position was chosen, and the mouse swam until it found the platform, or after 60 s was guided to the platform. The mouse was then allowed to stay on the platform for 15 s before being picked up (training trial). Twenty-four hours after the last training trial, the mouse was given a probe test without the platform. In this test, the mouse was placed in the pool once and allowed to search for 120 s. The time spent within the quadrant where the platform had previously been was recorded using an Ethovision XT (Noldus, Wageningen, Netherlands) video camera-based system.

Novel object-recognition test

A given mouse was placed in the open-field apparatus. All mice were habituated to the apparatus (without objects) for 15 min prior to the training session. At the end of each trial, the mouse was removed from the arena, and the arena was cleaned with 70% ethanol solution and dried with paper towels. Object recognition was scored by the amount of time spent with each object (defined as time spent with the nose of the mouse directed to the object and/or with its forelimbs touching the object). In the training session (T1: 10 min), two similar objects (left and right: cubes) were placed in a symmetrical position 5 cm away from the wall. In the retention session (T2: 10 min), two dissimilar objects were presented [one being a cube (right), as before, and the other a new one, a cylinder (left)]. The time spent exploring each object was recorded during T1 and during T2. All mice were tested with 24 h between T1 and T2. Just after the training session in the novel object-recognition test, 2 μL of PBS or recombinant human GPNMB (50 ng dissolved in PBS) was administered intracerebroventricularly under isoflurane anesthesia.

Passive-avoidance test

Conditions were determined by following a previously published procedure (Oyagi *et al.* 2012). Thirty minutes before the training trial, 0.1 mg/kg MK-801 (Sigma-Aldrich, St Louis, MO, USA) was intraperitoneally administered. Immediately after the training trial, 2 μL of PBS or recombinant human GPNMB (5 or 50 ng dissolved in PBS) was administered intracerebroventricularly under isoflurane anesthesia.

Mice were tested using a two-compartment box fitted with a foot-shock grid (Neuroscience, Tokyo, Japan). On the habituation day, a given mouse was placed into the lit compartment, facing away from the dark compartment, and allowed to explore for 30 s. After 30 s, the door was raised and the mouse was allowed to explore freely. Once the mouse entered the dark compartment with all four paws, the guillotine door was closed, and the mouse was removed and returned to the home cage 30 s later. On the training day (24 h after habituation), the mouse was again placed in the lit compartment, facing away from the dark compartment, and allowed to explore for 30 s. After 30 s, the guillotine door was lifted. As before, once the mouse had entered the dark compartment with all four paws, the guillotine door was closed. This time, the latency to enter was recorded (from the time the door was lifted). Three seconds after the door was closed, a foot-shock (0.25 mA, 2 s duration) was delivered. Thirty seconds after the foot-shock, the mouse was returned to its home cage. On the test day (24 h after training), the mouse was returned to the lit compartment, again facing away from the dark compartment, 30 s later the guillotine door was lifted. Again, once the mouse had entered the dark compartment with all four paws, the guillotine door was closed, and the latency to enter the dark compartment was recorded (from the time the door was lifted). No foot-shock was delivered. The mouse was removed and returned to its home cage. Animals that failed to enter the dark compartment within 1200 s were assigned a maximum latency score of 1200 s.

Western blot analysis

Mice were decapitated, brains quickly removed from the skull, briefly washed in ice-cold saline, laid on a cooled (4°C) metal plate, and hippocampi rapidly dissected out. These samples were homogenized in 10 mL/g radio-immunoprecipitation assay buffer (Sigma) supplemented with protease inhibitor cocktail (Sigma) and phosphate inhibitor cocktails 2 and 3 (Sigma). Lysates were centrifuged at 9170 *g* for 20 min at 4°C. To obtain a cell-membrane extract, fractionation was performed using a commercially available kit (Plasma membrane extraction kit; Abcam, Cambridge, MA, USA). An aliquot of 10 μg of protein was subjected to 5–20% sodium dodecyl sulfate–polyacrylamide gel electrophoresis, with the separated protein being transferred onto a polyvinylidene difluoride membrane (Immobilon-P; Millipore). For immunoblotting, the following primary antibodies were used: goat anti-GPNMB polyclonal antibody, rabbit anti-AMPA-selective glutamate receptor 1 (GluA1) polyclonal antibody (1 : 1000; Signalway Antibody, College Park, MD, USA), rabbit anti-phospho-GluA1 (Ser 845) polyclonal antibody (1 : 1000; Millipore), rabbit anti-phospho-glycogen synthase kinase3β (GSK3β) (Ser 9) monoclonal antibody (1 : 1000; Cell Signaling, Danvers, MA, USA), rabbit anti-GSK3β monoclonal antibody (1 : 1000; Cell Signaling), rabbit anti-phospho-Ca^{2+}/calmodulin-dependent protein kinase 2α (CaMK2α) (Thr 286) polyclonal antibody (1 : 1000; Santa Cruz Biotechnology, Santa Cruz, CA, USA), rabbit anti-CaMK2 polyclonal antibody (1 : 1000; Santa Cruz Biotechnology), rabbit anti-GluRε1 (NR2A) polyclonal antibody (1 : 1000; Frontier Science, Ishikari, Japan), rabbit anti-GluR1ζ (NR1) polyclonal antibody (1 : 1000; Frontier Science), rabbit anti-GluRε2 (NR2B) polyclonal antibody (1 : 1000; Frontier Science), and mouse anti-β-actin monoclonal antibody (1 : 5000; Santa Cruz Biotechnology). Secondary antibodies were as follows: horseradish peroxidase (HRP)-conjugated rabbit anti-goat IgG (1 : 4000; Thermo Scientific, Waltham, MA, USA), HRP-conjugated goat anti-mouse IgG (1 : 4000; Thermo

Scientific), or HRP-conjugated goat anti-rabbit IgG (1 : 4000, Thermo Scientific). Immunoreactive bands were visualized using ImmunoStar® LD (Wako Pure Chemical). Band intensity was measured using an LAS-4000 UV mini Luminescent Image Analyzer (Fujifilm, Tokyo, Japan) and Multi Gauge Version 3.0 (Fujifilm). For quantitative analysis, total protein signals were used as loading controls for phosphoprotein signals.

Electrophysiology

Hippocampal slices from Tg and ICR mice were prepared as described previously (Moriguchi *et al.* 2008). Recombinant human GPNMB (final concentration, 0.25 μg/mL) was introduced 20 min before high-frequency stimulation.

Transverse slices (400 μm thickness), prepared using a Vibratome microslicer (Microslicer DTK-1000; Dosaka, Kyoto, Japan), were incubated for 2 h in continuously oxygenized (95% O_2, 5% CO_2) artificial cerebrospinal fluid at 28°C. After a 2 h recovery period, a single slice was transferred to an interface recording chamber and perfused at a flow rate of 2 mL/min with artificial cerebrospinal fluid warmed to 34°C. Field excitatory post-synaptic potentials (fEPSPs) were evoked with a 0.05 Hz test stimulus through a bipolar stimulating electrode placed on the Schaffer collateral/commissural pathway, and they were recorded from the stratum radiatum of CA1 using a glass electrode filled with 3 M NaCl. Recording was performed using a single-electrode amplifier (CEZ-3100; Nihon Kohden, Tokyo, Japan), and the maximal value of the initial field excitatory post-synaptic potential slope was recorded and averaged every 1 min (3 traces) using an A/D converter (PowerLab 200; AD Instruments Pty Ltd., Sydney, NSW, Australia) and a personal computer. After a stable baseline was obtained, high-frequency stimulation at 100 Hz frequency and 1 s duration was applied twice with a 10 s interval, with test stimuli continuing for the indicated periods.

Statistical analysis

All data are expressed as the mean ± SEM. Statistical comparisons were performed using one-way ANOVA followed by Student's *t*-test, Dunnett's test, or Tukey's test. For data analysis, a two-way ANOVA followed by a *post hoc* multiple comparison test was used. Student's *t*-test was used to analyze the difference between two groups. A two-way ANOVA was used to analyze differences between groups (Figs 2(a), 4(b), 6(b) and (e), Figure S5). Dunnett's *post hoc* test was used to determine potential differences in the passive-avoidance test (Fig. 4a). A value of $p < 0.05$ was considered statistically significant. In the Results section, statistical analysis was by Student's *t*-test, except where noted.

Results

GPNMB is over-expressed in hippocampal neurons and astrocytes in GPNMB Tg mice

To investigate the effects of GPNMB on brain function, we used transgenic mice over-expressing GPNMB. Expression of GPNMB was confirmed by western blot analysis of extracts from the hippocampus, cortex, and striatum. The results showed that GPNMB protein

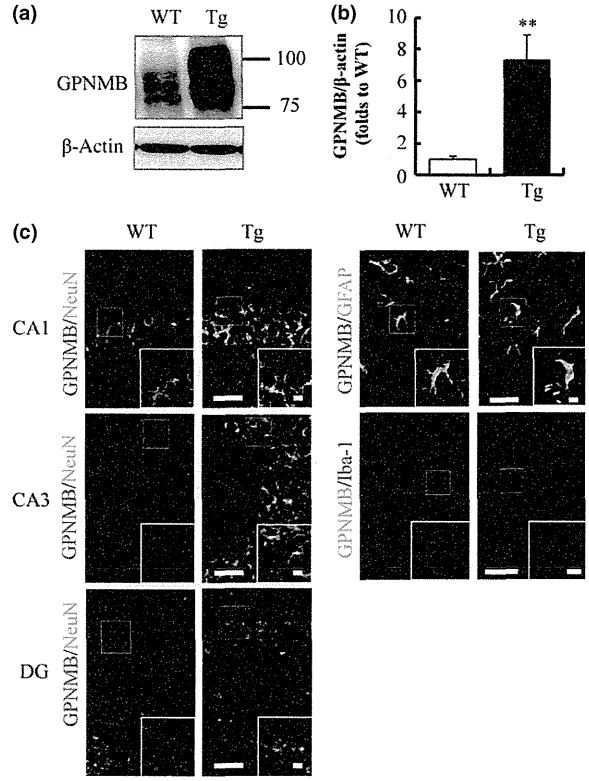

Fig. 1 Glycoprotein nonmelanoma protein B (GPNMB) is over-expressed in hippocampal neurons and astrocytes in GPNMB Tg mice. (a and b) Western blot analyses of GPNMB expression in hippocampus. (a) Representative images of immunoblots obtained using antibodies against GPNMB and β-actin. Results are shown for the hippocampus of WT and Tg mice. (b) Quantitative analyses of hippocampal GPNMB in WT and Tg mice. Data are expressed as mean fold difference versus WT mice (± SEM). $p = 0.007$, $^{**}p < 0.01$ versus WT mice, Student's *t*-test ($n = 6$). (c) Immunohistochemical analyses for the hippocampus of WT and Tg mice. Double immunostaining with antibodies against GPNMB, NeuN, glial fibrillary acidic protein (GFAP), and Iba-1 in CA1, CA3, and dentate gyrus (DG) regions, and in astrocytes, in WT and Tg mice. Scale bar = 40 μm (low-magnification views) or 10 μm (high-magnification views; shown at the bottom right of each panel).

expression in each extract was higher in Tg mice than in control WT mice [(hippocampus; $p = 0.007$, $n = 6$, Fig. 1a and b), (cortex; $p = 0.003$, $n = 4$, striatum; $p = 0.0003$, $n = 3$ or 4, Figure S1a and b)]. In the immunohistochemical analyses of brain sections, GPNMB expression was observed in neurons of the CA1, CA3, and dentate gyrus regions of the hippocampus, and also in GFAP-positive astrocytes but not in Iba-1-positive microglia within the hippocampus. GPNMB was also expressed in the cortex and striatum. In Tg mice, GPNMB was localized to the same sites as in WT mice (Fig. 1(c) and Figure S1c).

GPNMB over-expression does not influence spontaneous locomotor activity or anxiety-related responses

To investigate potential effects of GPNMB on general behavior in mice, we employed a locomotor-activity test and open-field test. We first performed a locomotor-activity test in the home cage, using WT and Tg mice, to assess the possible effects of GPNMB over-expression on circadian patterns of locomotor activity (Figure S2a and b). In this test, Tg mice exhibited no differences relative to WT mice [(total count; $p = 0.9$, day; $p = 0.5$, night; $p = 0.7$), WT; $n = 10$, Tg; $n = 9$]. We then performed an open-field test, in which WT and Tg littermates were indistinguishable. Indeed, there were no differences in the total distance moved ($p = 0.1$, $n = 10$) or in the time spent in the central area ($p = 0.7$, $n = 10$) between the two genotypes (Figure S2c and d). These results indicate that GPNMB over-expression did not alter either exploratory activity or anxiety-related responses.

GPNMB over-expression improves memory in the Morris water-maze test and novel object-recognition test

Next, to investigate whether GPNMB might contribute to memory retention, we employed the Morris water-maze test and novel object-recognition test. In the former test, following daily training, Tg mice exhibited a lower latency to escape than WT mice [genotype; $F(1, 30) = 4.300$, $p = 0.04$, time; $F(4, 120) = 2.367$, $p = 0.06$, genotype × time; $F(4, 120) = 0{,}674$, $p = 0.6$, two-way ANOVA with repeated measures] (Fig. 2a). In a probe test, Tg mice spent significantly more time in the target quadrant (where the platform was previously located) than WT mice ($p = 0.04$, WT; $n = 15$, Tg; $n = 16$, Fig. 2b and c). There was no significant difference between the two genotypes in either swimming velocity [$p = 0.6$, WT; 25.7 ± 1.6 cm/s ($n = 15$), Tg = 24.6 ± 1.1 cm/s ($n = 16$)] or distance traveled [$p = 0.5$, WT; 29.7 ± 1.8 m ($n = 15$), Tg = 28.2 ± 1.3 m ($n = 16$)] (Figure S3a and b). These results suggest that Tg mice exhibit improved performance relative to that of WT mice in terms of learning and retention kinetics of reference memory.

We also performed a novel object-recognition test, which assesses the animal's non-spatial memory of a novel object in a familiar setting. In the training session, no significant difference in exploratory time spent at the objects was observed between the two genotypes ($p = 0.1$, WT; $n = 6$, Tg; $n = 7$). In the retention session, both WT and Tg mice spent more time at the novel object than at the familiar object. However, Tg mice spent significantly more time at the novel object than WT mice ($p = 0.03$, WT; $n = 6$, Tg; $n = 7$, Fig. 2d). No significant difference in total exploration time was found between the two genotypes ($p = 0.3$, WT; 38.3 ± 10.0, Tg; 26.1 ± 5.8, $n = 6$ or 7, Fig. 2c).

We also performed a passive-avoidance test. In the training session, there were no obvious changes in distress vocalizations or reactions at the time of foot-shock delivery between Tg and WT mice. In the test session, the latency to enter the dark compartment was significantly lower in Tg mice than in WT mice ($p = 0.04$, WT; $n = 6$, Tg; $n = 9$, Fig. 2e). In the passive-avoidance test, Tg mice exhibited memory impairments. Further investigations using various trials will be needed to clarify the mechanisms mediating these contrary results.

Mechanisms underlying GPNMB-mediated improved memory retention in GPNMB Tg mice

To determine what might be responsible for the improvements in memory in Tg mice, we assessed the expression of various proteins in the hippocampus, since glutamate receptor expression levels in the hippocampus are associated with memory function (Tang *et al.* 1999; Reisel *et al.* 2002). Western blots were performed using unfractionated homogenates, which revealed increased levels of phosphorylated GluA1 (Ser 845) ($p = 0.02$, $n = 6$ or 7) and CaMK2α (Thr 286) in Tg mice ($p = 0.003$, $n = 6$), as well as increased total GluA1 expression ($p = 0.0004$, $n = 7$) (Fig. 3a and b). Protein levels of phosphorylated CaMK2α were increased ($p = 0.02$, $n = 6$), while total CaMK2α was unchanged ($p = 0.7$, $n = 6$) (Fig. 3a and b). GSK3β has been reported to regulate the insertion of GluA1-containing AMPA receptors into the plasma membrane (Du *et al.* 2010; Wei *et al.* 2010), and we found that levels of phosphorylated GSK3β (Ser 9) were higher in Tg mice ($p = 0.03$, $n = 6$ or 7, Fig. 3a and b). Both phosphorylated and total GSK3β were unchanged when normalized to β-actin [p-GSK3/β-actin ($p = 0.2$, $n = 7$), t-GSK3/β-actin ($p = 0.8$, $n = 7$)] (Fig. 3a and b). However, neither NMDA receptor subunit expression [NR2B ($p = 0.3$, WT; 1.0 ± 0.2, Tg; 0.8 ± 0.1, $n = 6$), NR2A ($p = 0.4$, WT; 1.0 ± 0.1, Tg; 0.9 ± 0.1, $n = 6$), NR1 expression ($p = 0.5$, WT; 1.0 ± 0.1, Tg; 0.9 ± 0.1, $n = 6$)] differed between Tg and WT mice (Figure S4).

The extracellular fragment of GPNMB improves memory retrieval

GPNMB is cleaved by extracellular proteinases resulting in the release of ECF (Rose *et al.* 2010), which then mediates angiogenesis and osteoblast differentiation (Selim *et al.* 2007; Rose *et al.* 2010). In the present study, we tested whether ECF, exogenously administered into the cerebral ventricles of ICR mice, modulates learning and memory. To evaluate the effects of ECF on memory retrieval, we used a recombinant human GPNMB consisting of only the ECF sequence. First, we performed a passive-avoidance test. The latency cutoff time was set at 1,200 s. In the retention test session, i.c.v. injection of ECF at 50 ng, but not at 5 ng, significantly increased the latency to enter the dark compartment (ECF 5 ng-treated group vs. PBS-treated group, $p = 0.5$; ECF 50 ng-treated group vs. PBS-treated group, $p = 0.01$, Dunnett's test, $n = 10$ or 11) (Fig. 4a). Intracerebroventricular injections were performed immediately after

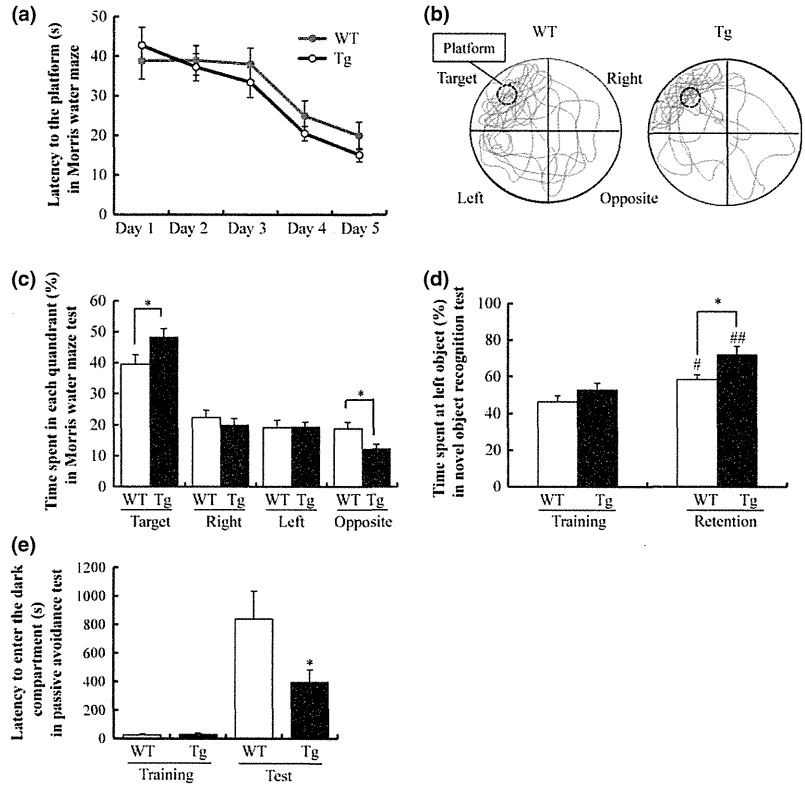

Fig. 2 Glycoprotein nonmelanoma protein B (GPNMB) Tg mice exhibit memory improvements in the Morris water-maze test and in a novel object-recognition test but memory impairment in a passive-avoidance test. (a and b) Morris water-maze test. (a) Latency to escape in WT and Tg mice in the training session. Genotype; $F(1, 30) = 4.300$, $p = 0.04$, time; $F(4, 120) = 2.367$, $p = 0.06$, genotype × time; $F(4, 120) = 0.674$, $p = 0.6$, two-way ANOVA with repeated measures. (b) Traces for WT and Tg mice in the probe test. (c) Time spent in each quadrant by WT and Tg mice in the probe test. Data are expressed as means ± SEM; $p = 0.04$, $^{*}p < 0.05$ versus WT mice, Student's *t*-test ($n = 15$ or 16). (d) Novel object-recognition test. Time spent at the left object by WT and Tg mice in the training and retention sessions. Data are expressed as mean time spent at the left object ± SEM. Training; $p = 0.1$, retention; $p = 0.03$, $^{*}p < 0.05$ versus WT mice; $^{\#}p < 0.05$, $^{\#\#}p < 0.01$ versus training session, Student's *t*-test ($n = 6$ or 7). (e) Passive-avoidance test. Latency to enter the dark compartment in each group in the training and test sessions. Data are expressed as mean latency ± SEM; $p = 0.04$, $^{*}p < 0.05$ versus WT mice, Student's *t*-test ($n = 5$ or 8).

the training session. Twenty-four hours after the retention test session, we performed an open-field test to assess the effect of the two doses of ECF on spontaneous locomotor activity. In this test, no significant differences in the total distance moved were observed among the groups by at least48 h after injection ($p = 0.9$, Dunnett's test, $n = 10$ or 11, Fig. 5). In addition, i.c.v. injection of 50 ng ECF showed a tendency to improve memory impairment induced by MK-801 (0.1 mg/kg, i.p.) treatment (data not shown). Intracerebroventricular injections were performed immediately after the training session. Furthermore, to clarify the effect of ECF treatment on both genotypes, we performed a novel object-recognition test. In the training session, the exploratory time spent at the objects was not significantly different among groups. In the retention session, i.c.v. treatment with 50 ng ECF significantly increased the time spent at the novel object ($p = 0.002$, $n = 6$ or 7, vs. PBS-treated WT group) (Fig. 4b). However, statistically significant differences were not observed following treatment with ECF ($p = 0.06$, Tg + PBS; 77.7 ± 2.2%, Tg + ECF; 86.7 ± 3.7%, $n = 6$). This result did not allow us to conclude with the necessary confidence that there were genotype-specific differences in the effects of ECF. Statistical analysis by two-way ANOVA revealed a significant effect of treatment [$F(1, 23) = 18.66$, $p = 0.0003$], but genotype [$F(1, 23) = 1.74$, $p = 0.200$] and the genotype × treatment interaction were not significant [$F(1, 23) = 2.09$, $p = 0.16$]. Further studies are required to understand the interactions between genotype and ECF administration, since improved memory retention was observed.

The extracellular fragment of GPNMB increases hippocampal GluA1 protein expression

Next, we evaluated the effect of ECF on glutamate receptor function by western blot analysis. ECF (50 ng; i.c.v.) was

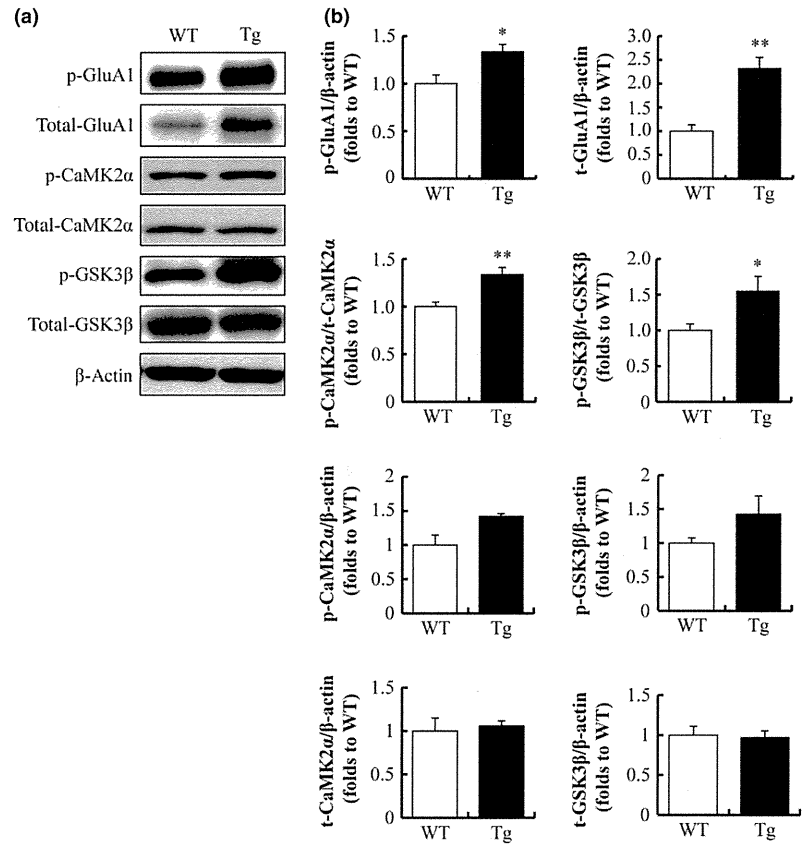

Fig. 3 Phosphorylation and expression levels of various proteins in the hippocampus of glycoprotein nonmelanoma protein B (GPNMB) Tg mice. (a) Representative image of immunoblots obtained from WT and Tg mice by using antibodies against phosphorylated GluA1 (Ser 845) (p-GluA1), GluA1, phosphorylated CaMK2α (Thr286) (p-CaMK2α), CaMK2α, phosphorylated glycogen synthase kinase 3β (GSK3β) (Ser 9) (p-GSK3β), GSK3β, and β-actin. (b) Quantitative analyses for p-GluA1, GluA1, p-CaMK2α, p-GSK3β, and β-actin. Numbers are normalized against control values. Data are expressed as mean fold difference versus WT mice (± SEM), p-GluA1; $p = 0.02$, p-CaMK2α; $p = 0.003$, t-GluA1; $p = 0.0004$, p-GSK3β; $^{*}p = 0.03$, $^{**}p < 0.05$, 0.01 versus WT mice, Student's *t*-test ($n = 6$ or 7).

administered to ICR mice within 10 min of the passive-avoidance test training session. Mice were sacrificed 24 h after ECF administration, and hippocampal extracts were examined. Western blots were performed using unfractionated homogenates, except for Fig. 5c and d where hippocampal homogenates were fractionated to obtain cell-membrane fractions. Immunoblotting analyses revealed higher levels of GluA1 in the total-cell and cell-membrane extracts in the ECF-treated group than in either the naive group or PBS-treated group ($p = 0.02$, Fig. 5a and b). By contrast, levels of phosphorylated CaMK2α (Thr 286), GluA1 (Ser 845), and GSK3β (Ser 9) were not different among these groups [p-GluA1/β-actin ($p = 0.5$, $n = 9$–10), p-CaMK2α/CaMK2α ($p = 0.8$, $n = 10$), p-CaMK2α/β-actin ($p = 0.5$, $n = 10$), t-CaMK2α/β-actin ($p = 0.8$, $n = 10$), p-GSK3β/t-GSK3β($p = 1.0$, $n = 10$), p-GSK3β/β-actin ($p = 0.4$, $n = 9$), t-GSK3β/β-actin ($p = 1.0$, $n = 9$), Fig. 5a and b]. Similarly, GluA1 mRNA expression did not differ [ECF vs. PBS; 1 h ($p = 0.8$), 3 h ($p = 1$), 6 h ($p = 0.2$), 12 h ($p = 1$), 24 h ($p = 0.8$), $n = 3$, Figure S6]. Interestingly, GluA1 protein levels in membrane fractions (as validated by the expression of epidermal growth factor receptor (EGFR) and absence of Histone H1) were increased by ECF treatment ($p = 0.003$, $n = 3$, Fig. 5c and d). In Fig. 5(c) and (d), we investigated whether the increase in GluA1 expression originated from increased GluA1 expression in membrane fractions. Notably, GluA1 expression was increased in membrane fractions, which indicates that the amount of available AMPA receptors might also be increased. In Fig. 5(e) and (f), we investigated the expression of total GluA1 protein in whole cells obtained from Tg mice, in contrast to the results of Fig. 5(a) and (b). However, ECF treatment did not affect the expression of GluA1 in Tg mice ($p = 0.5$, $n = 3$, Fig. 5e and f).

The extracellular fragment of GPNMB facilitates long-term potentiation

To clarify whether GPNMB influences long-term synaptic plasticity, we investigated its effect on hippocampal LTP, which is widely regarded as a cellular model of learning and memory. Immediately after stimulation, the degree of LTP was significantly higher in Tg mice than in WT control mice [1 min; $p = 0.03$, (WT; 198.8 ± 6.9, Tg; 238.0 ± 13.2), 60 min; $p = 0.3$, (WT; 157.7 ± 4.4, Tg; 170.4 ± 9.9), $n = 5$, Fig. 6a–c]. Statistical analysis by two-way ANOVA revealed a significant effect of genotype [$F(1, 59) = 83.9$, $p < 0.001$]. In ECF (0.25 μg/mL)-treated hippocampal slices, LTP was significantly increased 60 min after stimulation

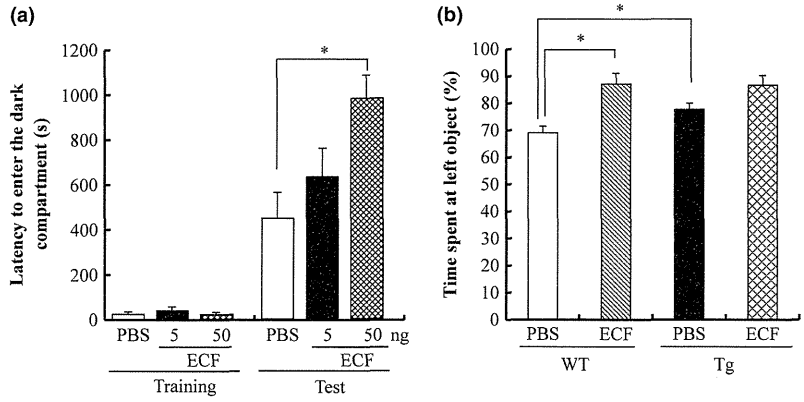

Fig. 4 The extracellular fragment of glycoprotein nonmelanoma protein B (GPNMB) (ECF) influences memory retrieval. (a) Results from the passive-avoidance test obtained 24 h after treatment with one of two doses of the ECF of GPNMB (i.c.v.). Latency to enter the dark compartment in each group in the training and test sessions. Intracerebroventricular injections were performed immediately after the training session. Data are expressed as mean latency ± SEM; $p = 0.01$, $^*p < 0.05$ versus Phosphate-buffered saline (PBS)-treated group, Dunnett's test ($n = 10$ or 11). (b) Results from the novel object-recognition test. Data are expressed as mean exploration time ± SEM; $p = 0.06$, Tg + PBS; 77.7 ± 2.2%, Tg + ECF; 86.7 ± 3.7%, Student's *t*-test ($n = 6$).

compared to that of the PBS-treated control [1 min; $p = 0.2$, (WT; 221.6 ± 8.3, Tg; 247.9 ± 17.4), 60 min; $p = 0.05$ (WT; 152.1 ± 13, Tg; 201.8 ± 16.8), $n = 5$, Fig. 6d–f]. Statistical analysis by two-way ANOVA revealed that the effect of GPNMB ECF application was significant [$F(59, 480) = 5.6, p < 0.001$]. These results suggested that GPNMB over-expression and GPNMB ECF application promote LTP, which might play an important role during memory formation.

Discussion

The present study, using mice, is the first to demonstrate that GPNMB improves both spatial and non-spatial memory. In addition, it revealed that ECF is sufficient to induce both memory improvements and increase expression of the AMPA receptor subunit GluA1 in the hippocampus.

A recent study demonstrated localization of GPNMB in neurons, microglia, and radial glia, but not in astrocytes, within the rat hippocampus (Huang *et al.* 2012). Here, we detected GPNMB in neurons and also in GFAP-positive astrocytes but not in Iba-1- positive microglia (Fig. 1c). The explanation for this discrepancy may lie in the differences in species, methods, and/or antibodies used. The reason why GPNMB was expressed in both neurons and astrocytes is unclear. However, the ECF experiments suggest that GPNMB might perform similar functions in both neurons and astrocytes and that extracellular GPNMB might affect memory functions in an autocrine or paracrine manner. Previous reports demonstrate that intact transmembrane GPNMB is cleaved by extracellular proteases, such as matrix metalloproteinases including ADAM10, which results in the release of the extracellular domain to act as a growth factor or cytokine (Furochi *et al.* 2007a). In addition, we showed that the ECF of GPNMB improved memory (Fig. 4). Therefore, GPNMB may function as a secretory protein.

The Morris water-maze test and the novel object-recognition test are used to evaluate spatial and non-spatial memory, respectively (Denayer *et al.* 2008; Okun *et al.* 2010). In these tests, Tg mice displayed improvements in both spatial and non-spatial memory (Fig. 2a–d).

In addition, we found that ECF improved memory (Fig. 4). These results reveal an ability of GPNMB to improve hippocampus-dependent memory and suggest that ECF may contribute to such memory improvements. Contrary to expectations, Tg mice exhibited memory impairments in a passive-avoidance test (Fig. 2e).

We further investigated the mechanisms underlying memory improvements in Tg mice and ECF-treated mice. The results showed increased hippocampal levels of GluA1, the essential subunit of the AMPA receptor, in both Tg mice and ECF-treated mice, together with increased levels of the phosphorylated forms of GluA1, CaMK2α, and GSK3β in the hippocampus of Tg mice, but not ECF-treated mice (Figs 3, 5a and b). ECF was administered during memory retrieval, which occurred immediately after the acquisition trial in both the passive-avoidance test and novel object-recognition test. Further studies are required to reveal the detailed effects of GPNMB ECF, although ECF may affect memory retrieval.

Finally, in the investigation of LTP, GPNMB Tg mice exhibited promotion of LTP compared with that of WT mice, although only slightly (Fig. 6b). Moreover, GPNMB ECF-treated hippocampal slices also exhibited promotion of LTP (Fig. 6e). However, total GluA1 expression was increased in

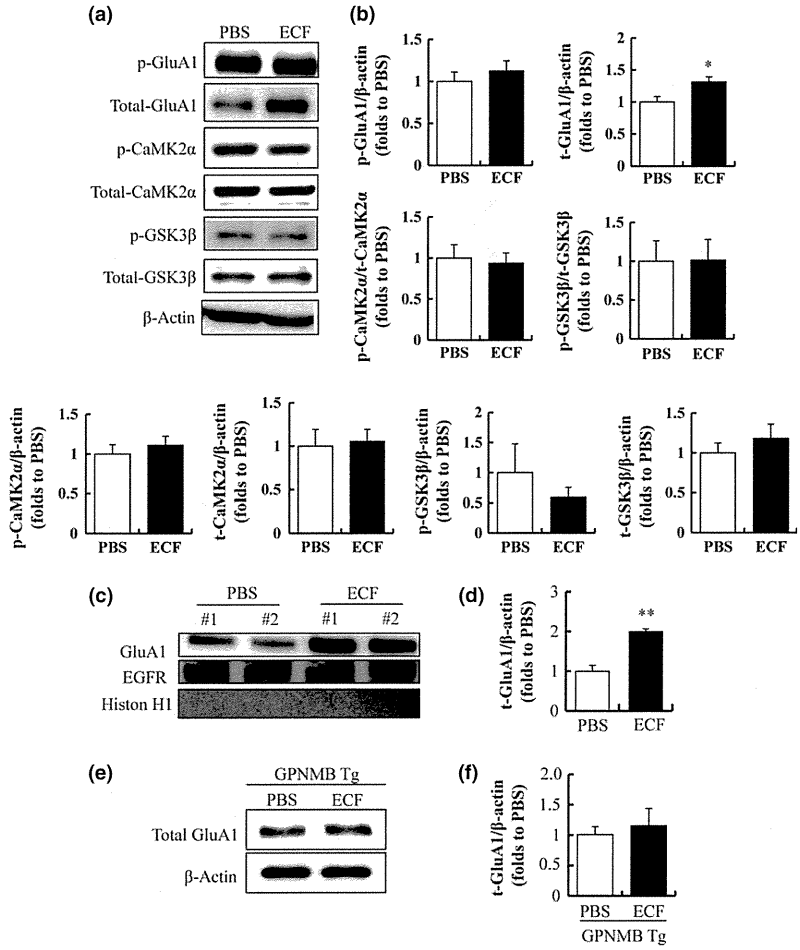

Fig. 5 Treatment with the glycoprotein nonmelanoma protein B (GPNMB) ECF modulates hippocampal effects of training in the passive-avoidance test. (a and b) Western blot analyses of hippocampal total cell extracts from phosphate-buffered saline (PBS)-treated or extracellular fragment of GPNMB (ECF)-treated groups 24 h after treatment. (a) Representative image of immunoblots obtained using antibodies against p-GluA1, GluA1, p-CaMK2α, CaMK2α, p-GSK3β, GSK3β, and β-actin. (b) Quantitative analyses for p-GluA1, GluA1, p-CaMK2α, p-GSK3β, and β-actin. Data are expressed as mean fold difference versus PBS-treated group (± SEM); p-GluA1/β-actin ($p = 0.5$, vehicle; 1.1 ± 0.7, ECF; 1.2 ± 0.2, $n = 9$–10), p-CaMK2α/CaMK2α ($p = 0.8$, vehicle; 1.1 ± 0.2, ECF; 1.0 ± 0.1, $n = 10$), p-GSK3β/GSK3β ($p = 0.97$, vehicle; 1.0 ± 0.3, ECF; 1.0 ± 0.3, $n = 10$), $^{*}p < 0.05$ versus PBS-treated group, Student's *t*-test ($n = 9$ or 10). (c and d) Western blot analyses of hippocampal membrane extracts obtained from PBS-treated and ECF of GPNMB-treated groups 24 h after treatment. (c) Representative image of immunoblots obtained using antibodies against GluA1, EGFR, and Histone H1. Proteins in the membrane fraction were detected. (d) Quantitative analyses of GluA1 surface expression. Data are expressed as mean fold difference versus PBS-treated group (± SEM); $p = 0.003$, $^{**}p < 0.01$ versus PBS-treated group, Student's *t*-test ($n = 3$). (e and f) Western blot analyses of hippocampal tissue obtained from PBS-treated or extracellular fragment of GPNMB-treated GPNMB Tg mice 24 h after treatment. ECF did not affect GluA1 protein levels in GPNMB Tg mice. (e) Representative image of immunoblots obtained using antibodies against GluA1 and β-actin. GluA1 protein levels in the hippocampus were measured by western blotting 24 h after treatment with PBS or ECF (50 ng) in GPNMB Tg mice. (f) Quantitative analyses for GluA1 and β-actin. Data are expressed as mean fold difference versus PBS-treated group (± SEM) ($n = 3$), $p = 0.5$, Student's *t*-test.

both the hippocampus of Tg and ECF-treated mice (Figs 3 and 5). These results suggested that GPNMB might increase the amount of available AMPA receptors, leading to improved memory formation via the promotion of LTP.

We hypothesize that such an increase in GluA1 expression may lead to an increase in the overall expression of AMPA receptors present in the hippocampus, followed by an increase in membrane depolarization through AMPA receptors and the subsequent opening of voltage-dependent Ca^{2+} channels. Phosphorylation of GluA1 by CaMK2 or cAMP-dependent protein kinase regulates AMPA receptor function by two different mechanisms: modulation of

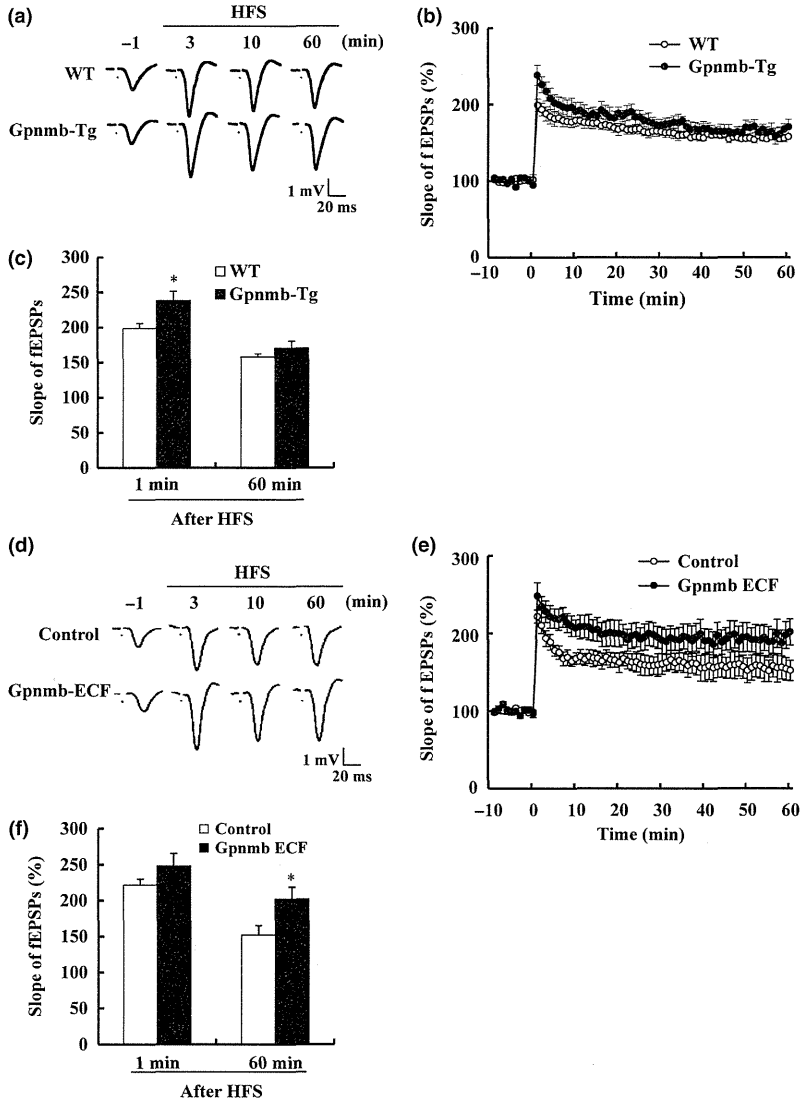

Fig. 6 Effects of glycoprotein nonmelanoma protein B (GPNMB) on the induction of long-term potentiation (LTP). (a–c) LTP results in Tg mice (a) Representative field excitatory post-synaptic potentials (fEPSPs) from the CA1 region of Tg and WT mice. (b) Change-in-slope data for fEPSPs following high-frequency stimulation (HFS) in the CA1 region in slices obtained from Tg and WT mice. (c) Levels of LTP at 1 and at 60 min after HFS in the CA1 region. Values are means ± SEM, 1 min; $p = 0.03$, (WT; 198.8 ± 6.9, Tg; 238.0 ± 13.2), 60 min; $p = 0.3$, (WT; 157.7 ± 4.4, Tg; 170.4 ± 9.9), $^*p < 0.05$ versus WT mice, Student's *t*-test ($n = 5$). (d–f) Effect of extracellular fragment (ECF) on LTP (d) Representative fEPSPs from the CA1 region. (e) Change-in-slope data for fEPSPs following HFS in the CA1 region in slices treated with ECF or vehicle. (f) Levels of LTP at 1 and 60 min after HFS in the CA1 region. Values are means ± SEM, 1 min; $p = 0.2$, (WT; 221.6 ± 8.3, Tg; 247.9 ± 17.4), 60 min; $p = 0.05$ (WT; 152.1 ± 13, Tg; 201.8 ± 16.8), $^*p < 0.05$ versus control, Student's *t*-test ($n = 5$).

channel properties (Kristensen *et al.* 2011) and trafficking of AMPA receptors to the cell surface (Hayashi *et al.* 2000; Passafaro *et al.* 2001). Furthermore, both CaMK2 and GSK3β are phosphorylated during the induction of LTP, and serve to modulate the insertion of AMPA receptors into the cell surface (Peineau *et al.* 2007; Du *et al.* 2010; Lisman *et al.* 2012). The level of phosphorylation of these proteins seems to reflect GluA1 expression levels, and presumably the subsequent GluA1-mediated calcium influx. On that basis, GPNMB levels and the consequent GluA1 expression levels might account for the differences between Tg mice and ECF-treated mice. By contrast, no differences in NMDA receptor subunit expression (NR2B, NR2A, and NR1) or dendritic spine density were observed in the hippocampus of Tg and WT mice (Figures S3 and S4). These results indicate that GPNMB released from neurons and astrocytes may improve memory by selectively facilitating the function and expression of AMPA receptors in the hippocampus.

Through ectodomain shedding, intact transmembrane GPNMB is cleaved into three fragments with molecular masses of approximately 90 and 100 kDa (ECF), 20 kDa (intracellular fragment I), and 14 kDa (intracellular fragment II), as shown in C2C12 myoblasts by Furochi *et al.* (2007a). Since GPNMB contains an Arg-Gly-Asp motif in the ECF, the mechanism of action of GPNMB may involve secreted GPNMB acting as an extracellular matrix protein and binding to integrins and to an integrin-syndecan-4 complex (Sheng *et al.* 2008; Chung *et al.* 2009). Integrins are heterodimeric extracellular matrix protein receptors that are widely expressed throughout the nervous system. Moreover, integrin β1 is associated with AMPA receptor-mediated synaptic transmission (Chan *et al.* 2006). Furthermore, treatment with peptides containing an Arg-Gly-Asp integrin

β1-binding motif promotes LTP in hippocampal preparations (Xiao *et al.* 1991). Although we did not identify the receptor that binds the ECF of GPNMB, we postulate that integrin β1 signaling might partially contribute to the function of GPNMB. Increased GluA1 and AMPA receptors expression may explain the effects of the GPNMB ECF. However, further experiments are required to clarify the mechanisms mediating the actions of GPNMB.

In conclusion, the present study demonstrated that both GPNMB Tg mice and ECF-treated mice exhibited improved memory in learning tasks. In addition, GPNMB increased hippocampal GluA1 levels and available AMPA receptors, and promoted LTP in Tg mice and ECF-treated mice. Our findings suggest that these behavioral and synaptic improvements may be associated with increased hippocampal GluA1, GSK3β, and CaMKII protein expression. Moreover, these results suggest that GPNMB may be a novel target for further research on higher order brain functions such as memory.

Acknowledgments and conflict of interest disclosure

The authors have no conflicts of interest to declare.

All experiments were conducted in compliance with the ARRIVE guidelines.

Supporting information

Additional supporting information may be found in the online version of this article at the publisher's web-site:

Appendix S1. Supplementary Materials and methods.

Figure S1. GPNMB is over-expressed in the cortex and striatum of GPNMB Tg mice.

Figure S2. GPNMB Tg mice exhibit normal behavior in the locomotor-activity test and open-field test.

Figure S3. Activity levels in memory-related behavioral tests.

Figure S4. NMDA receptor expression levels.

Figure S5. The GPNMB extracellular fragment does not affect spontaneous locomotor activity.

Figure S6. ECF does not affect GluA1 expression at the transcriptional level.

References

Chan C. S., Weeber E. J., Zong L., Fuchs E., Sweatt J. D. and Davis R. L. (2006) Beta 1-integrins are required for hippocampal AMPA receptor-dependent synaptic transmission, synaptic plasticity, and working memory. *J. Neurosci.* **26**, 223–232.

Chung J. S., Bonkobara M., Tomihari M., Cruz P. D., Jr and Ariizumi K. (2009) The DC-HIL/syndecan-4 pathway inhibits human allogeneic T-cell responses. *Eur. J. Immunol.* **39**, 965–974.

Denayer E., Ahmed T., Brems H. *et al.* (2008) Spred1 is required for synaptic plasticity and hippocampus-dependent learning. *J. Neurosci.* **28**, 14443–14449.

Du J., Wei Y., Liu L. *et al.* (2010) A kinesin signaling complex mediates the ability of GSK-3beta to affect mood-associated behaviors. *Proc. Natl Acad. Sci. USA* **107**, 11573–11578.

Furochi H., Tamura S., Mameoka M. *et al.* (2007a) Osteoactivin fragments produced by ectodomain shedding induce MMP-3 expression via ERK pathway in mouse NIH-3T3 fibroblasts. *FEBS Lett.* **581**, 5743–5750.

Furochi H., Tamura S., Takeshima K., Hirasaka K., Nakao R., Kishi K. and Nikawa T. (2007b) Overexpression of osteoactivin protects skeletal muscle from severe degeneration caused by long-term denervation in mice. *J. Med. Invest.* **54**, 248–254.

Haralanova-Ilieva B., Ramadori G. and Armbrust T. (2005) Expression of osteoactivin in rat and human liver and isolated rat liver cells. *J. Hepatol.* **42**, 565–572.

Hayashi Y., Shi S. H., Esteban J. A., Piccini A., Poncer J. C. and Malinow R. (2000) Driving AMPA receptors into synapses by LTP and CaMKII: requirement for GluR1 and PDZ domain interaction. *Science* **287**, 2262–2267.

Huang J. J., Ma W. J. and Yokoyama S. (2012) Expression and immunolocalization of Gpnmb, a glioma-associated glycoprotein, in normal and inflamed central nervous systems of adult rats. *Brain Behav.* **2**, 85–96.

Huovila A. P., Turner A. J., Pelto-Huikko M., Karkkainen I. and Ortiz R. M. (2005) Shedding light on ADAM metalloproteinases. *Trends Biochem. Sci.* **30**, 413–422.

Kristensen A. S., Jenkins M. A., Banke T. G., Schousboe A., Makino Y., Johnson R. C., Huganir R. and Traynelis S. F. (2011) Mechanism of Ca2+/calmodulin-dependent kinase II regulation of AMPA receptor gating. *Nat. Neurosci.* **14**, 727–735.

Lisman J., Yasuda R. and Raghavachari S. (2012) Mechanisms of CaMKII action in long-term potentiation. *Nat. Rev.* **13**, 169–182.

Makino H. and Malinow R. (2009) AMPA receptor incorporation into synapses during LTP: the role of lateral movement and exocytosis. *Neuron* **64**, 381–390.

Mitsushima D., Ishihara K., Sano A., Kessels H. W. and Takahashi T. (2011) Contextual learning requires synaptic AMPA receptor delivery in the hippocampus. *Proc Natl Acad Sci U S A*, **108**, 12503–12508.

Moriguchi S., Shioda N., Han F., Narahashi T. and Fukunaga K. (2008) CaM kinase II and protein kinase C activations mediate enhancement of long-term potentiation by nefiracetam in the rat hippocampal CA1 region. *J. Neurochem.* **106**, 1092–1103.

Ogawa T., Nikawa T., Furochi H. *et al.* (2005) Osteoactivin upregulates expression of MMP-3 and MMP-9 in fibroblasts infiltrated into denervated skeletal muscle in mice. *Am. J. Physiol.* **289**, C697–C707.

Okun E., Griffioen K., Barak B. *et al.* (2010) Toll-like receptor 3 inhibits memory retention and constrains adult hippocampal neurogenesis. *Proc. Natl Acad. Sci. USA* **107**, 15625–15630.

Oyagi A., Oida Y., Kakefuda K. *et al.* (2009) Generation and characterization of conditional heparin-binding EGF-like growth factor knockout mice. *PLoS ONE* **4**, e7461.

Oyagi A., Moriguchi S., Nitta A., Murata K., Oida Y., Tsuruma K., Shimazawa M., Fukunaga K. and Hara H. (2012) Heparin-binding EGF-like growth factor is required for synaptic plasticity and memory formation. *Brain Res.* **1419**, 97–104.

Passafaro M., Piech V. and Sheng M. (2001) Subunit-specific temporal and spatial patterns of AMPA receptor exocytosis in hippocampal neurons. *Nat. Neurosci.* **4**, 917–926.

Peineau S., Taghibiglou C., Bradley C. *et al.* (2007) LTP inhibits LTD in the hippocampus via regulation of GSK3beta. *Neuron* **53**, 703–717.

Plagnol V. N. M., Bras J. M., Hernandez D. G. *et al.* (2011) A two-stage meta-analysis identifies several new loci for Parkinson's disease. *PLoS Genet.* **7**, e1002142.

Reisel D., Bannerman D. M., Schmitt W. B., Deacon R. M., Flint J., Borchardt T., Seeburg P. H. and Rawlins J. N. (2002) Spatial

memory dissociations in mice lacking GluR1. *Nat. Neurosci.* **5**, 868–873.

Rose A. A., Annis M. G., Dong Z., Pepin F., Hallett M., Park M. and Siegel P. M. (2010) ADAM10 releases a soluble form of the GPNMB/Osteoactivin extracellular domain with angiogenic properties. *PLoS ONE* **5**, e12093.

Ruoslahti E. (1996) RGD and other recognition sequences for integrins. *Annu. Rev. Cell Dev. Biol.* **12**, 697–715.

Safadi F. F., Xu J., Smock S. L., Rico M. C., Owen T. A. and Popoff S. N. (2001) Cloning and characterization of osteoactivin, a novel cDNA expressed in osteoblasts. *J. Cell. Biochem.* **84**, 12–26.

Schwarzbich M. A., Gutknecht M., Salih J., Salih H. R., Brossart P., Rittig S. M. and Grunebach F. (2012) The immune inhibitory receptor osteoactivin is upregulated in monocyte-derived dendritic cells by BCR-ABL tyrosine kinase inhibitors. *Cancer Immunol. Immunother.* **61**, 193–202.

Selim A. A., Castaneda J. L., Owen T. A., Popoff S. N. and Safadi F. F. (2007) The role of osteoactivin-derived peptides in osteoblast differentiation. *Med. Sci. Monit.* **13**, BR259–BR270.

Sheng M. H., Wergedal J. E., Mohan S. and Lau K. H. (2008) Osteoactivin is a novel osteoclastic protein and plays a key role in osteoclast differentiation and activity. *FEBS Lett.* **582**, 1451–1458.

Smith A. M. and Wehner J. M. (2002) Aniracetam improves contextual fear conditioning and increases hippocampal gamma-PKC activation in DBA/2J mice. *Hippocampus* **12**, 76–85.

Tanaka H., Shimazawa M., Kimura M. *et al.* (2012) The potential of GPNMB as novel neuroprotective factor in amyotrophic lateral sclerosis. *Sci. Rep.* **2**, 573.

Tang Y. P., Shimizu E., Dube G. R., Rampon C., Kerchner G. A., Zhuo M., Liu G. and Tsien J. Z. (1999) Genetic enhancement of learning and memory in mice. *Nature* **401**, 63–69.

Wei J., Liu W. and Yan Z. (2010) Regulation of AMPA receptor trafficking and function by glycogen synthase kinase 3. *J. Biol. Chem.* **285**, 26369–26376.

Xiao P., Bahr B. A., Staubli U., Vanderklish P. W. and Lynch G. (1991) Evidence that matrix recognition contributes to stabilization but not induction of LTP. *NeuroReport* **2**, 461–464.

STEM CELLS TRANSLATIONAL MEDICINE®

TISSUE-SPECIFIC PROGENITOR AND STEM CELLS

Progranulin, a Major Secreted Protein of Mouse Adipose-Derived Stem Cells, Inhibits Light-Induced Retinal Degeneration

KAZUHIRO TSURUMA,[a,*] MIKA YAMAUCHI,[a,*] SOU SUGITANI,[a] TOMOHIRO OTSUKA,[a] YUTA OHNO,[a] YUKI NAGAHARA,[a] YUKA IKEGAME,[b] MASAMITSU SHIMAZAWA,[a] SHINICHI YOSHIMURA,[b] TORU IWAMA,[b] HIDEAKI HARA[a]

Key Words. Progranulin • Adipose-derived stem cell • Photoreceptor • Retina • Light-induced photoreceptor cell death

[a]Department of Biofunctional Evaluation, Molecular Pharmacology, Gifu Pharmaceutical University, Gifu, Japan; [b]Department of Neurosurgery, Gifu University Graduate School of Medicine, Gifu, Japan

[*]Contributed equally as first authors.

Correspondence: Hideaki Hara, Ph.D., Department of Biofunctional Evaluation, Molecular Pharmacology, Gifu Pharmaceutical University, 1-25-4 Daigaku-nishi, Gifu 501-1196, Japan. Telephone: 81-58-230-8126; E-Mail: hidehara@gifu-pu.ac.jp

Received February 5, 2013; accepted for publication August 6, 2013; first published online in SCTM *Express* November 14, 2013.

1066-5099/2013/$20.00/0

http://dx.doi.org/10.5966/sctm.2013-0020

ABSTRACT

Adipose tissue stromal vascular fraction contains mesenchymal stem cells, which show protective effects when administered to damaged tissues, mainly through secreted trophic factors. We examined the protective effects of adipose-derived stem cells (ASCs) and ASC-conditioned medium (ASC-CM) against retinal damage and identified the neuroprotective factors in ASC-CM. ASCs and mature adipocytes were isolated from mouse subcutaneous tissue. ASCs were injected intravitreally in a mouse model of light-induced retinal damage, and ASC injection recovered retinal function as measured by electroretinogram and inhibited outer nuclear layer, thinning, without engraftment of ASCs. ASC-CM and mature adipocyte-conditioned medium were collected after 72 hours of culture. In vitro, H_2O_2- and light-induced cell death was reduced in a photoreceptor cell line with ASC-CM but not with mature adipocyte-conditioned medium. In vivo, light-induced photoreceptor damage was evaluated by measurement of outer nuclear layer thickness at 5 days after light exposure and by electroretinogram recording. ASC-CM significantly inhibited photoreceptor degeneration and retinal dysfunction after light exposure. Progranulin was identified as a major secreted protein of ASCs that showed protective effects against retinal damage in vitro and in vivo. Furthermore, progranulin phosphorylated extracellular signal-regulated kinase, cAMP response element binding protein, and hepatocyte growth factor receptor, and protein kinase C signaling pathways were involved in the protective effects of progranulin. These findings suggest that ASC-CM and progranulin have neuroprotective effects in the light-induced retinal-damage model. Progranulin may be a potential target for the treatment of the degenerative diseases of the retina. STEM CELLS TRANSLATIONAL MEDICINE *2014;3:42–53*

INTRODUCTION

Excessive light exposure leads to photoreceptor degeneration [1], and several epidemiological studies have suggested that long-term history of exposure to light may have some impact on the incidence of age-related macular degeneration [2]. Photoreceptor loss is the primary cause of blindness in degenerative diseases such as age-related macular degeneration and retinitis pigmentosa. However, there are few effective therapeutic strategies for these diseases. Therefore, meaningful therapeutic methods such as transplantation, regenerative therapy, and photoreceptor-protective agents are required.

Recently, transplanted bone marrow-derived stem cells (BMSCs) have been shown to exert significant neuroprotection in several central nervous system degenerative models [3–6]. In the retina, intravitreal BMSC transplantation resulted in a significant decrease in the rate of retinal ganglion cell axon loss normalized to cumulative intraocular pressure exposure [7]. BMSC transplantation could inhibit photoreceptor apoptosis and slow down retinal damage in light-damaged rat eyes [8]. Despite the improvements observed, only a few integrated into the neural retina, and the majority of the transplanted cells survived in the vitreous cavity because of glial reactivity. Moreover, no engrafted cells differentiated into neural or retinal cells [7–9]. It is possible that these improvements are the result of trophic support provided to host cells from factors released by mesenchymal stem cells (MSCs).

Adipose-derived stem cells (ASCs) are MSCs within the subcutaneous adipose tissue that self-renew and display multilineage developmental plasticity [10, 11]. ASCs can be obtained repeatedly in large quantities under local anesthesia. A comparative analysis of MSCs obtained from bone marrow, adipose tissue, and umbilical cord clearly showed no differences between MSCs and ASCs in terms of morphology, immune phenotype, colony frequency, and differentiation capacity [12, 13].

ASCs secrete several potentially beneficial growth factors such as vascular endothelial growth factor, hepatocyte growth factor (HGF), basic fibroblast growth factor, and insulin-like growth factor 1 [14, 15], which may protect retinal neurons from injury as well as promote endogenous repair. Some evidence supports the protective effect of cytokines during oxidative stress; for example, basic fibroblast growth factor has been shown to protect photoreceptor cells from light-induced retinal damage in mice [16], and HGF has been shown to have protective effects against retinal ischemia-reperfusion [17]. These reports indicate the retinal protective effects of stem cells and cytokines. Recently, we have reported that ASC-conditioned medium (ASC-CM) has a neuronal protective effect [18]. Therefore, we evaluated the protective effects of ASCs and ASC-CM against retinal degeneration in vitro and in vivo and the various factors included in ASC-CM.

Progranulin is a 593-amino-acid, cysteine-rich protein that was originally identified as the precursor of smaller related peptides, referred to as "granulin." Progranulin is expressed in a variety of peripheral tissues as well as in the adult central nervous system, including cortical and hippocampal pyramidal cells [19]. It is particularly prominent in epithelial and hematopoietic cells and tends to be more highly expressed in tissues with high turnover rates [20, 21]. Moreover, progranulin also promotes tumor cell invasiveness [22–24], and it is upregulated during wound healing and stimulates neutrophil, macrophage infiltration, and neovascularization of wound tissue [25, 26]. In the central nervous system, mutations in progranulin have been reported to cause tau-negative frontotemporal dementia, showing the important function of progranulin in neuronal survival [27]. Neurons from progranulin-deficient mice were more vulnerable to damage by activated microglia and by depletion of oxygen and glucose [28]. Recently, tumor necrosis factor (TNF) receptors have been revealed to be receptors for progranulin [29]. In the retina, "progranulin-a" was expressed in microglia at the site of light-induced photoreceptor injury in zebrafish [30]. Consequently, progranulin may play an important role in retinal neuroprotection.

In the present study, we identified progranulin as a major secreted factor from ASC-CM and examined the protective effects of ASC-CM and progranulin against retinal damage in vitro and in vivo.

Materials and Methods

Animals

Male adult ddY mice and C57BL/6-Tg (CAG-EGFP) mice were purchased from Japan SLC, Inc. (Hamamatsu, Japan, http://www.jslc.co.jp/). They were kept under controlled lighting conditions (12-hour light/12-hour dark). Nine- or 10-week-old ddY mice were used in the experiments. All experiments were performed in accordance with the Association for Research in Vision and Ophthalmology Statement for the Use of Animals in Ophthalmic and Vision Research and were approved and monitored by the institutional animal care and use committee of Gifu Pharmaceutical University.

Isolation and Culture of ASCs and Mature Adipocytes

Murine ASCs were obtained from a C57BL/6-Tg (CAG-EGFP) mouse that ubiquitously expresses enhanced green fluorescent protein (EGFP). Cells were obtained from a 16-week-old female mouse.

Adipose tissue was dissected from a subcutaneous site. For ASC harvest, the inguinal fat pads were removed, and a cell pellet containing ASCs was obtained, as described previously [31]. Briefly, the fat tissue was minced, digested with 0.15% collagenase (Wako Pure Chemical Industries, Ltd., Osaka, Japan, http://www.wako-chem.co.jp/egaiyo/), and centrifuged. After this procedure, most of the mature adipocytes remained in the supernatant. The floating adipocytes were collected and washed twice in Dulbecco's modified Eagle's medium (DMEM; Sigma-Aldrich, St. Louis, MO, http://www.sigmaaldrich.com). The cell pellet was resuspended in 10% fetal bovine serum (FBS)/DMEM and plated in a 100-mm culture dish. ASCs were maintained in 10% FBS/DMEM, 100 U/ml penicillin (Meiji Seika Pharma Co., Ltd., Tokyo, Japan, http://www.meiji-seika-pharma.co.jp/english/index.html), and 100 μg/ml streptomycin (Meiji Seika) under a humidified atmosphere of 95% air and 5% carbon dioxide (CO_2) at 37°C. The cells were passaged by trypsinization every 3–4 days and were used in the experiments from passages 4–8. ASCs were characterized by MSC markers and a leukocyte marker (supplemental online Fig. 1). The multipotency of ASCs was confirmed, as described in our previous report [31].

Collection of ASC-CM and Mature Adipocyte-Conditioned Medium

ASCs and mature adipocytes (4×10^5 cells) were cultured in FBS-free DMEM. ASC-CM and mature adipocyte-conditioned medium were collected after 72 hours of culture, centrifuged at 300*g* for 5 minutes, and filtered using a 0.22-μm syringe filter. The media were concentrated by centrifugation at 2,600*g* using the Amicon Ultra-15 (Millipore, Billerica, MA, http://www.millipore.com; molecular weight cutoff: 3,000).

Cell Culture

Mouse photoreceptor-derived 661W cells were a kind gift from Dr. Muayyad R. Al-Ubaidi (Department of Cell Biology, University of Oklahoma Health Sciences Center, Oklahoma City, OK). The cells were maintained in 10% FBS/DMEM, 100 U/ml penicillin, and 100 μg/ml streptomycin under a humidified atmosphere of 95% air and 5% CO_2 at 37°C. The cells were passaged by trypsinization every 3–4 days and were used in the experiments from passage 5 to passage 15.

H_2O_2-Induced and Light-Induced Cell Death in 661W Cell Cultures

The 661W cells were seeded at 2×10^3 (H_2O_2 study) or 3×10^3 (light irradiation study) cells per well in 96-well plates and then incubated for 24 hours. The medium of the experimental groups was then replaced with 1% FBS ASC-CM, and the cells were incubated for 12 hours. Recombinant mouse progranulin (R&D Systems Inc., Minneapolis, MN, http://www.rndsystems.com) was dissolved in phosphate buffered saline (PBS) and added to the medium. Pretreatment with 100 μM Trolox (Sigma-Aldrich), a vitamin E analog and an antioxidant regent, was done as a positive control. Then, H_2O_2 (Wako) was added at a final concentration of 0.3 mM. Nuclear staining assays were carried out after 27 hours. In the light-induced cell death assay, at 1 hour before progranulin treatment, the cells were treated with U0126 (Promega, Madison, WI, http://www.promega.com), a mitogen-activated protein/extracellular signal-regulated kinase kinase inhibitor, H-89 (Merck & Co., Whitehouse Station, NY, http://www.merck.com), a protein

kinase A inhibitor, and Gö 6976 (Merck), a protein kinase C (PKC) inhibitor. Thereafter, the cells, in the absence or presence of ASC-CM or recombinant mouse progranulin, were exposed to 2,500 lux (lx) of light using a white fluorescent lamp (Nikon, Tokyo, Japan, http://www.nikon.com) for 24 hours under a humidified atmosphere of 95% air and 5% CO_2 at 37¡C. The luminance was measured using a light meter LM-332 (As One Corporation, Osaka, Japan, http://www.as-1.co.jp/), and the temperature of the cell surface was measured using a noncontact thermometer MT-7 (As One). Dark control cells and light-stressed 661W cells were all from the same stock, eliminating any preexisting bias (e.g., light, temperature). as previously described by Kanan et al. [32]. The experiments were always started at around 9 a.m. Nuclear staining assays were carried out after light exposure.

Hoechst 33342 and Propidium Iodide Staining

Cell death was observed by using combination staining with two fluorescent dyes, Hoechst 33342 and propidium iodide (PI; both from Invitrogen, Carlsbad, CA, http://www.invitrogen.com). At the end of the culture period, Hoechst 33342 and PI were added to the culture medium for 15 minutes at final concentrations of 8.1 μM and 1.5 μM, respectively. Images were collected using an Olympus IX70 inverted epifluorescence microscope (Olympus, Tokyo, Japan, http://www.olympus-global.com). The total number of cells (not fewer than 500 cells in each group) was counted in a blind manner (M.Y.), and the percentage of PI-positive cells was calculated.

Cytokine Array

RayBio Biotin Label-based Mouse Antibody Array I (RayBiotech, Inc., Norcross, GA, http://www.raybiotech.com) was used to investigate cytokines secreted by ASCs. Briefly, the membranes were blocked with blocking buffer and then incubated with biotin-labeled medium from ASCs or mature adipocytes cultures at room temperature for 2 hours. The membranes were washed, horseradish peroxidase-conjugated streptavidin was added, and the membranes were incubated at room temperature for 2 hours. The membranes were developed by using enhanced chemiluminescence-type solution and visualized using a LAS-4000 luminescent image analyzer (Fuji Film, Tokyo, Japan, http://www.fujifilm.com/).

Western Blot Analysis

ASC-CM was supplemented with protease inhibitor cocktail (Sigma-Aldrich), phosphate inhibitor cocktails 2 and 3 (Sigma-Aldrich), and sample buffer (Wako). In vitro, 661W cells were washed with PBS, harvested, and lysed in RIPA buffer (Sigma-Aldrich) supplemented with protease inhibitor cocktail and phosphate inhibitor cocktails 2 and 3. Lysates were centrifuged at 12,000*g* for 15 minutes at 4°C. Protein concentrations were measured by comparison with a known concentration of bovine serum albumin, using a bicinchoninic acid protein assay kit. Thereafter, sample buffer was added and boiled for 5 minutes. The samples were subjected to 5%–20% sodium dodecyl sulfate polyacrylamide gel electrophoresis and then transferred onto polyvinylidene difluoride membranes (Immobilon-P; Millipore). For immunoblotting, the following primary antibodies were used: monoclonal anti-mouse progranulin antibody (R&D Systems), anti-β-actin, (Sigma-Aldrich), anti-ERK1/2, anti-phosphorylated ERK1/2, anti-HGF receptor (MET), anti-phosphorylated MET (Cell Signaling Technology, Danvers, MA, http://www.cellsignal.com), anti-cAMP response element binding protein (Cell Signaling Technology), and anti-phosphorylated CREB (Santa Cruz Biotechnology, Inc., Santa Cruz, CA, http://www.scbt.com). The primary antibodies were diluted 1:1,000 using Can Get Signal Solution 1 (Toyobo, Osaka, Japan, http://www.toyobo.co.jp/e), and incubated for overnight at 4°C. Anti-mouse or anti-rabbit horseradish peroxidase-conjugated secondary antibody was used. The secondary antibodies were diluted 1:2,000 using Can Get Signal Solution 2 (Toyobo) and incubated for 45 minutes at room temperature. The immunoreactive bands were visualized using Immunostar-LD (Wako) and an LAS-4000 luminescent image analyzer.

Confirmation of ASC Intravitreous Injection

Mice were anesthetized with 3.0% isoflurane (Merck Animal Health, Boxmeer, The Netherlands, http://www.merck-animal-health.com/) and maintained with 1.5% isoflurane in 70% nitrous oxide and 30% oxygen by an animal general anesthesia apparatus (Soft Lander; Sin-ei Industry Co., Ltd., Saitama, Japan, http://www.shinei.me). ASCs (1×10^3 cells per eye; total injected volume was 2 μl) contained in DMEM were then intravitreously injected in the left eyes. After 2 days of ASCs injection, ocular fundus images were obtained using a retinal imaging microscope (Micron III; Phoenix Research Laboratories Inc., Pleasanton, CA, http://www.phoenixreslabs.com/). Five microliters of ophthalmic solution containing 0.5% tropicamide and 0.5% phenylephrine hydrochloride (Mydrin-P; Santen, Osaka, Japan, http://www.santen.com/en/) was applied topically 10 minutes before anesthesia to dilate the pupil, and then mice were anesthetized intraperitoneally with a mixture of ketamine (120 mg/kg; Daiichi-Sankyo, Tokyo, Japan, http://www.daiichisankyo.com/) and xylazine (6 mg/kg; Bayer Health Care, Tokyo, Japan, http://www.bayer.com/en/Homepage.aspx). A few minutes later, 0.1% purified sodium hyaluronate (Hyalein; Santen) was applied topically to prevent desiccation and to keep the surface smooth, and fundus images were captured.

Exposure to Light

After dark adaptation for 24 hours, the pupils of the mice were dilated with 1% cyclopentolate hydrochloride eye drops (Santen) at 30 minutes before exposure to light. Nonanesthetized mice were exposed to 8,000 lx of white fluorescent light (Toshiba, Tokyo, Japan, https://www.toshiba.co.jp/worldwide/index.html) for 3 hours in cages with a reflective interior. The temperature during exposure to light was maintained at 25°C ± 1.5°C. After exposure to light, all mice were returned to darkness for 24 hours and then placed in a normal light/dark cycle.

ASCs (10^3 cells per eye) or DMEM (as a vehicle) was injected into the vitreous chamber of ddY mice at 24 hours after light exposure in order to avoid damage to ASCs by light. In addition, we prepared dead ASCs as a control for electroretinogram (ERG). ASCs were killed by heating at 80°C for 30 minutes and injected into the vitreous chamber. ASC-CM concentrated 150-fold or recombinant mouse progranulin (100 μg/ml) was intravitreally injected (1 μl per eye) at 6 hours before exposure to light.

ERG

ERGs were recorded at 5 days (ASC-CM injected group) or 27 days (ASC- or dead-ASC-injected group) after light exposure (Mayo,